[American Journal of Science, Vol. 322, February, 2022, P. 65–107, DOI 10.2475/02.2022.01]

American Journal of Science

FEBRUARY 2022

DETRITAL ZIRCON PROVENANCE OF THE ARCHEAN MOODIES GROUP, BARBERTON GREENSTONE BELT, SOUTH AFRICA AND ESWATINI

CHRISTOPH HEUBECK[*,†], NADJA DRABON[**], GARY BYERLY[***], ISABELLE LEISGANG[§,##], ULF LINNEMANN[§§], DON LOWE[§§§], REGINA MERTZ-KRAUS[§], ALEJANDRA GONZALEZ-PINZON[‡], TONNY B. THOMSEN[‡‡], ARMIN ZEH[‡‡‡], YAMIRKA ROJAS-AGRAMONTE[§,#], and ALFRED KRÖNER[§,¶]

ABSTRACT. Sandstones of the 3.22 Ga Archean Moodies Group represent one of the world's oldest quartz-rich sedimentary sequences. The provenance of this unit is unresolved because its quartz and common microcline can be sourced both from either now eroded or covered granitoid plutons outside the Barberton Greenstone Belt (BGB) or, alternatively and perhaps more controversially, (rhyo-)dacitic (sub-) volcanic rocks within the BGB.

We compiled 31 detrital zircon data sets (n = 2588) from sandstones, reworked tuffs and conglomerate of the Moodies Group in order to constrain its age and provenance. After selection using quality criteria, the remaining zircons (n = 1621) in nearly all samples show a distribution corresponding to the four known major pulses of felsic magmatism in the BGB: 1) the *ca.* 3550 to 3530 Ma Theespruit and Sandspruit Formations at the base of the Onverwacht Group; 2) the *ca.* 3440 to 3410 Ma rhyo-dacites of the upper Hooggenoeg Formation, Onverwacht Group; 3) the *ca.* 3300 to 3280 Ma thin felsic tuffs in the Mendon Formation; and 4) the *ca.* 3260 to 3215 Ma felsic volcanic and shallow intrusive rocks of the Auber Villiers, Bien Venue and Schoongezicht Formations of the upper Fig Tree Group and the Moodies Group as well as their co-magmatic plutonic counterparts. Almost all data sets also contain near-concordant younger zircons as young as 2820 Ma, which can be attributed to

[*] Institut für Geowissenschaften, Friedrich-Schiller-Universität Jena, Burgweg 11, 07749 Jena, Germany

[**] Department of Earth and Planetary Sciences, Harvard University, 20 Oxford St., Cambridge, Massachusetts 02138, USA

[***] Department of Geology and Geophysics, Louisiana State University, Baton Rouge, Louisiana 70803, USA

[§] Institut für Geowissenschaften, Johannes-Gutenberg-Universität, J.-J.-Becher-Weg 21, 55128 Mainz

[§§] Senckenberg Naturhistorische Sammlungen Dresden, Museum für Mineralogie und Geologie, Königsbrücker Landstraße 159, 01109 Dresden, Germany

[§§§] Department of Earth and Environmental Sciences, Stanford University, Braun Hall, Stanford, California 94305-2115, USA

[‡] Natural Colombia Mineral, Calle 137 # 12b-49, 112111 Bogotá, Colombia

[‡‡] Geological Survey of Denmark and Greenland (GEUS), Øster Voldgade 10, Copenhagen, Denmark

[‡‡‡] Institut für Angewandte Geowissenschaften, Mineralogie und Petrologie, Karlsruher Institut für Technologie (KIT), Adenauerring 20b, Geb. 50.40, 76131 Karlsruhe, Germany

[#] Institut für Geowissenschaften, Christian-Albrechts-Universität zu Kiel, Ludewig-Meyn-Straße 10, 24118 Kiel, Germany

[##] now at: Ingenieurfakultät Bau Geo Umwelt, Lehrstuhl für Ingenieurgeologie, Technische Universität München, Arcisstrasse 21, 80333 München, Germany

[¶] deceased

[†] corresponding author: christoph.heubeck@uni-jena.de

one of six tectonic or magmatic events affecting the young Kaapvaal Craton in post-BGB time, causing the partial or complete resetting of the U-Pb system in some grains. The youngest (near-)concordant zircon clusters yield ages of *ca.* 3220 Ma in most locations, and the youngest discordant group of zircons from a reworked tuff near the top of the Moodies Group at 3212 ± 13 Ma agrees well with previous estimates of the maximum depositional age. With very few exceptions, the oldest zircons (*ca.* 3564 Ma) are only slightly older than the oldest rocks in the BGB stratigraphy (*ca.* 3550 Ma). Subtle regional and stratigraphic differences in age spectra may indicate localized or nearby sediment sources within a synorogenic setting. Preliminary age spectra along vertical stratigraphic profiles show little systematic variation, possibly indicating that intrabasinal recycling was dominant over considerable time periods of the basin's evolution. Extra-basinal plutonic sources of similar age and composition as the intra-BGB sources appear to be required to provide quartz and some feldspar to Moodies Group sandstones, although zircon age spectra, limited zircon Hf isotope data, sandstone petrography, facies analysis, and the high variability in Moodies conglomerate clast composition are consistent with uplift, deformation and erosion of several intra-BGB sources, but in particular from the region of the Onverwacht Anticline. Zircon populations, conglomerate clasts, and sandstone composition show no evidence that high-grade metamorphic rocks from the adjacent Ancient Gneiss Complex (AGC) contributed significantly to the Moodies Group.

Key words: Zircon provenance, Tectonics, Barberton Greenstone Belt, Archaean, Detrital Zircons

INTRODUCTION

The origin, extent, growth rate and growth mechanisms of the early continental crust are fundamental questions and a widely debated issue in geosciences (Arndt and Nesbit, 2012; van Kranendonk and others, 2014, 2018; Kamber, 2015; Bedard, 2018; and many others). It is mostly addressed through a combination of geochemical, isotopic, structural-tectonic and stratigraphic studies. Part of this "toolbox" is the statistical analysis of detrital zircon ages from sedimentary units to shed light on the tectonic setting, provenance, and age of source regions no longer accessible because they are either buried or were eroded (Dickinson and Gehrels, 2009; Gehrels, 2014; Vermeesch, 2012).

In the context of early Earth geology, geochronological and geochemical studies of detrital zircon populations are commonly used to "look beyond" the stratigraphic age of the host sedimentary rock to infer the age and abundance (or rarity) of early continental crust and lithosphere-forming processes, the early temperature regime at the Earth's surface and the presence of oceans (Mojzsis and others, 2001; Wilde and others, 2001; Valley and others, 2002, 2005; Van Kranendonk and others, 2018; Kröner and others, 2019). The clastic sedimentary strata of greenstone belts in cratonic areas play a key role in these studies because they record surface processes, including the uplift, weathering and erosion of even older rocks.

In this contribution, we report the age spectra of detrital zircon grains from the Moodies Group of the Barberton Greenstone Belt (BGB), South Africa and Eswatini (formerly Swaziland; fig. 1), one of the oldest well-preserved quartz-rich units on Earth. Our aim is to constrain the provenance of the Moodies Group by compiling all available detrital zircon age data and to interpret them in the light of literature data from sandstone petrography, facies analysis, Hf isotopes, and regional geologic mapping. We will also use tuffs conformably interbedded with the sandstones to refine the depositional age of the Moodies Group and evaluate the significance of post-depositional zircon populations. It is not our intent to engage in a wide-ranging evaluation of tectonic models based on Moodies Group zircon provenance data because the available data set is too small and heterogeneous and because addressing this issue would

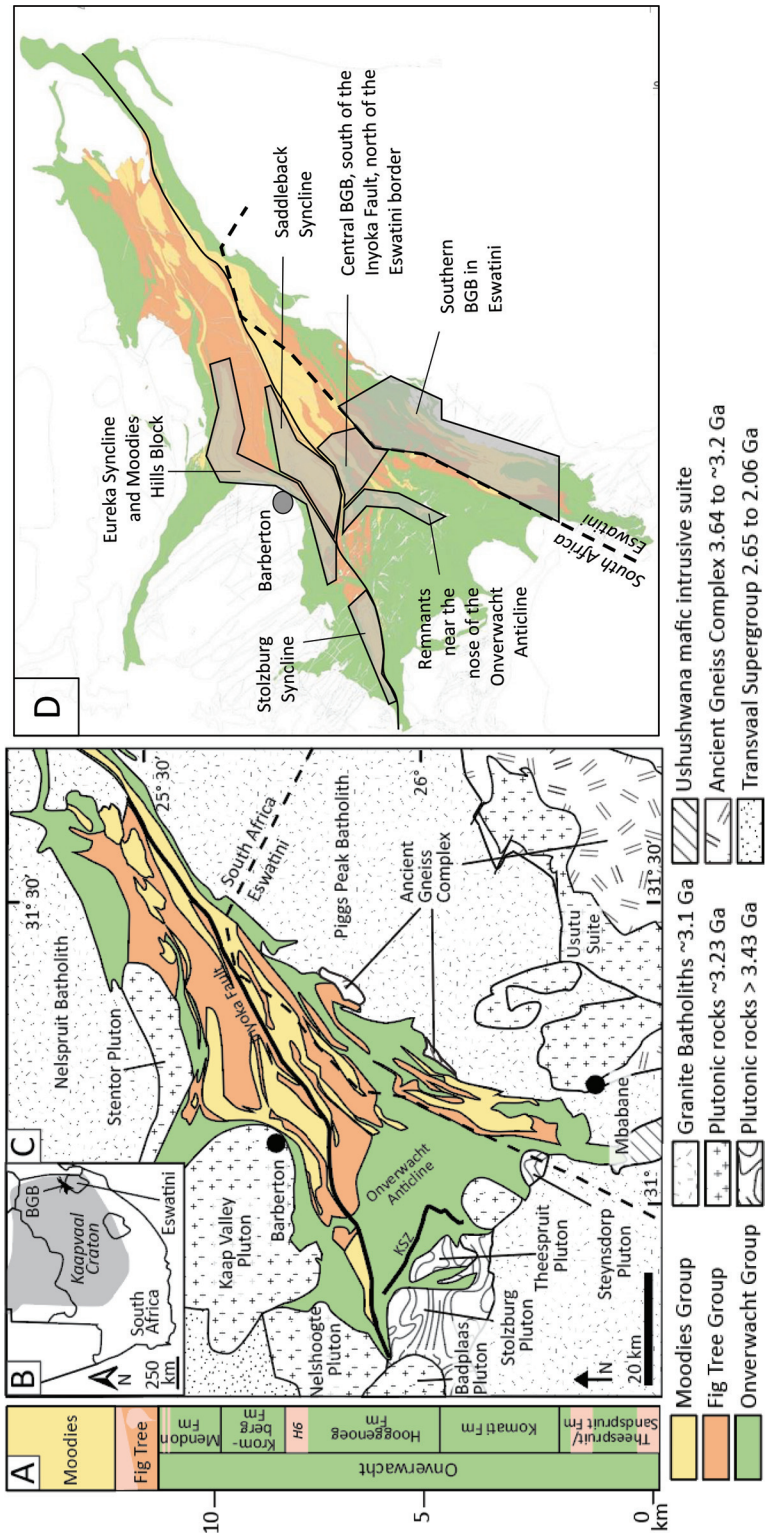

Fig. 1. Geology of the Barberton Greenstone Belt. (A): Stratigraphic column. Pink areas indicate phases of major felsic magmatism. (B): Inset map, showing the BGB at the eastern margin of the Early Archean Kaapvaal Craton. (C): Simplified geologic map. (D): Regions within the BGB by which detrital zircon age spectra are grouped (compare fig. 5A-F; table 1).

Fig. 2. View along strike looking towards the southwest in the north-central BGB, showing steeply-dipping and tightly-folded and faulted quartz-rich sandstones of the Moodies Group.

have required us to discuss diverse aspects of structural geology, stratigraphy, and geochemistry.

REGIONAL GEOLOGY

The Barberton Greenstone Belt (BGB) is the largest and best-preserved supracrustal unit in the basement of the Kaapvaal Craton (fig. 1). The Moodies Group is the uppermost and youngest unit of the Barberton Supergroup, the volcanic-sedimentary sequence forming the BGB.

The Moodies Group (fig. 2) predominantly consists of immature to mature, fine- to coarse-grained, quartz-rich arkoses, subarkoses, litharenites and quartzarenites up to *ca.* 3.7 km thick, with significant conglomerates and siltstones and minor volcanic rocks and ferruginous sediments.

Moodies strata were deposited, in part syn-deformationally, in alluvial, fluvial, deltaic, tidal and shallow-marine environments (review in Heubeck, 2019). Due to their thickness and facies variety, preserved in stratigraphic and tectonic context, Moodies Group strata represent a unique record of a Paleoarchean marine-terrestrial transition. Abundant tidal-facies sandstones with microbial mats provide insights into the early shallow-water biosphere (Heubeck, 2009; Gamper and others, 2012; Homann and others, 2015). The quartz-dominated and in places feldspar-rich Moodies sandstones apparently mark large-scale access of surface systems to voluminous felsic igneous rocks.

Moodies Group strata crop-out over much of the BGB for *ca.* 110 km along strike and *ca.* 40 km width (figs. 1–4). The unit is variably bounded at its base by a gradual conformable contact at the top of the underlying Fig Tree Group, by unconformable

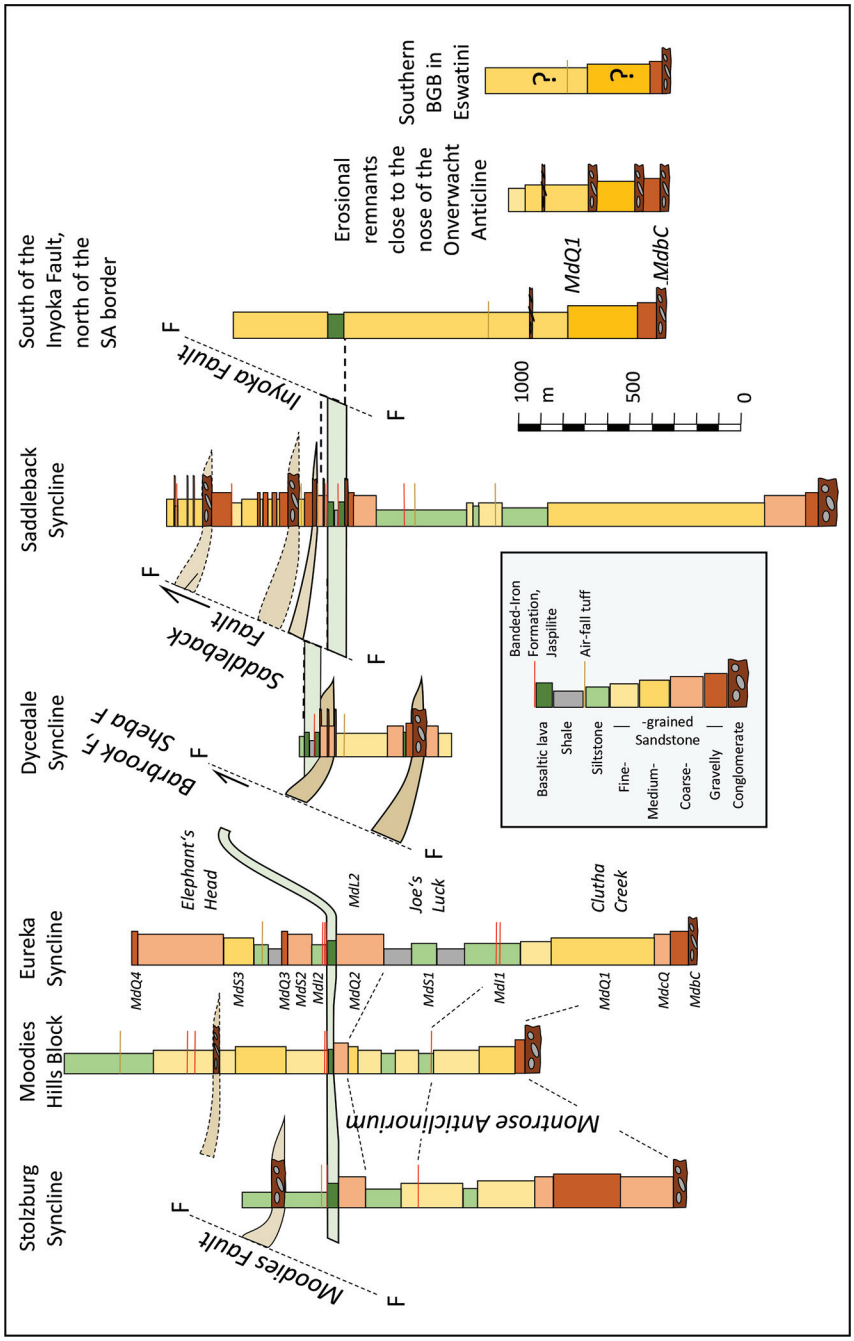

Fig. 3. Stratigraphic correlation diagram of Moodies Group lithologies and units between the major tectonic units in the BGB (fig. 1D), mostly north of the Inyoka Fault (modified from Heubeck, 2019). The top of the Moodies basaltic lava MdL2 serves as a stratigraphic datum, but offsets by major faults are recognized. The stratigraphy south of the Inyoka Fault is poorly known.

contacts to older rocks of the Fig Tree and Onverwacht groups, or by fault zones. Moodies strata are nowhere in stratigraphic contact with overlying younger rocks (fig. 1). Moodies Group strata differ on either side of the major, BGB-axial Inyoka Fault (figs. 1 and 3): Those north of the Inyoka Fault allow lithostratigraphic correlation among several tectonic blocks, whereas the Moodies Group in South Africa and Eswatini south of the Inyoka Fault is not well studied (Urie, 1970, 1971; Lamb, 1984; Lamb and Paris, 1988; Heubeck and Lowe, 1999; fig. 3). There, the group appears to be thinner (<2 km), to lack feldspar, and to have a higher metamorphic grade. It mostly consists, as far as is currently known, of thick, dominantly horizontally-stratified and cross-bedded quartzose sandstones and conglomerates.

Although the overall metamorphic grade of Moodies Group strata is only lower-greenschist facies (*ca.* 325–425°C) in most areas (Xie and others, 1997; Tice and others, 2004), BGB strata, including those of the Moodies Group, were also widely affected by syn-depositional hydrothermal alteration, burial metamorphism, and several tectonothermal events during the Archaean and the early Proterozoic. These events may have partially reset U-Pb systems in zircon. Mineral alteration, strain and metamorphic grade differ regionally; they are generally higher along the margins of the greenstone belt (Anhaeusser, 1972, 1976, 2019; Schmitz and Heubeck, 2021) and near major fault zones within the belt (Heubeck and Lowe, 1994). Ductile deformation appears to increase regionally towards the southeast where Moodies conglomerates are commonly highly strained (Schmitz and Heubeck, 2021).

Parts or all of the Moodies Group have been variously interpreted as a foreland basin with provenance from older crustal blocks (Jackson and others, 1987; Heubeck and Lowe, 1994), a synorogenic basin (de Wit, 1991), a passive margin overlying unexposed crystalline basement (Eriksson, 1979), an intramontane basin in an extensional setting (Heubeck and Lowe, 1994), or a uniquely Archean "sag basin" between rising plutons (Van Kranendonk, 2011; Van Kranendonk and others, 2009, 2014; Schmitz and Heubeck, 2021). The provenance of the Moodies Group is thus a matter of debate. Likely intra-BGB sources of sand-sized detritus include litharenites, cherts and banded iron formations from the underlying Fig Tree Group (2–3 km thick), and in particular the intermediate to felsic volcanic and juvenile shallow intrusive rocks of the Schoongezicht (Reimer, ms 1967; Lowe and Byerly, 1999), Auber Villiers (Lowe and Byerly, 1999) and Bien Venue (Kohler and Anhaeusser, 2002) Formations (*ca.* 3240–3225 Ma) (fig. 1). Volcanic strata of the Onverwacht Group, up to 11 km thick, which underlie the Fig Tree Group, may also have contributed. These, however, are dominated by mafic and ultramafic rocks and are unlikely to have produced abundant quartzose sand-sized material; only rhyodacites and related felsic volcanic rocks in the Sandspruit and Theespruit Formations of the basal Onverwacht Group, 3550 to 3520 Ma, in the H6 member of the Hooggenoeg Formation, *ca.* 3445 Ma, and some mostly thin, interbedded cherts throughout the Onverwacht Group would contribute to potent sources of quartz-rich sand.

Alternatively, potential external sources of sediment could have included the bimodal banded gneisses and granitoids of the Ancient Gneiss Complex in Eswatini (fig. 1) where some zircons are up to 90 Ma older than the oldest preserved strata in the BGB (Kröner and Compston, 1988; Kröner and others, 2018b), as well as the large plutonic tracts of TTG (tonalite-trondhjemite-granodiorite) composition surrounding the BGB (Moyen and others, 2018). Along these lines of thought, Heubeck and Lowe (1999) interpreted Moodies sediment provenance to represent first-time access of surface systems to exposed (crust-stabilizing) granitoids, resulting in the production of large quantities of coarse-grained monocrystalline quartz and K-feldspar grains.

PREVIOUS STUDIES

Several previous studies have addressed the provenance of the Moodies Group. Hessler and Lowe (2006) compiled petrographic data from all the sedimentary lithologies in the Moodies Group to study provenance and weathering regime. They argued that conglomerate clast composition and sandstone petrography tended to reflect contributions less prone to breakdown by mechanical and chemical weathering, such as quartz-rich felsic rocks and chert, whereas the mafic component was preferentially fractionated into Moodies Group siltstone and shale; the fine grain-size fraction also represented a better-averaged source of provenance information. Hessler and Lowe (2006) concluded that the provenance of the Moodies Group was dominated by tonalite, felsic volcanic rock, komatiite, basalt, and granite. Heubeck and Lowe (1999) focused on the stratigraphic evolution of sandstone composition north of the Inyoka Fault, defined petrofacies trends and postulated a mix of plutonic extra-BGB and various intra-BGB sources. Knauth and Lowe (2003; their fig. 5) documented a consistent trend to more positive $\delta^{18}O$ isotope values with increasing stratigraphic height, sampled from cherts from a >6 km thick section of the Onverwacht Group from the limbs of the Onverwacht Anticline. These authors found this isotopic trend inverted in conglomerate chert clasts of the overlying Fig Tree and Moodies Groups (Knauth and Lowe, 2003; their fig. 7), that is, $\delta^{18}O$ values decreased with increasing stratigraphic height. Knauth and Lowe (2003) interpreted this trend as being consistent with increasingly and progressively deeper erosion into the greenstone belt sequence.

The most comprehensive analysis of detrital zircons from the BGB was by Drabon and others (2017) who studied 21 sandstones of the Fig Tree and three samples of the Moodies Group (two additional samples were from transitional stratigraphic positions) and 27 samples from impact-derived spherule beds. Zeh and others (2013) compared detrital zircons and εHf isotope data from a Fig Tree greywacke and a Moodies sandstone sample with the compositions of surrounding crystalline rocks and inferred an overall southern provenance of Moodies zircons. Byerly and others (2018) analyzed 2033 zircons from two localities of the Green Sandstone Bed (Mendon Formation of the Onverwacht Group, *ca.* 3306 Ma) to document rare Hadean (>4000 Ma) zircons from the BGB. A dedicated and systematic, stratigraphically-controlled study of detrital zircon ages from Moodies strata is to-date lacking.

The Moodies basal conglomerate attracted geochronologic attention early (van Niekerk and Burger, 1978) because its clasts were recognized as messengers of even older, but now eroded or covered, rocks than those of the BGB. To date, rare granitoid clasts from the well-exposed, easily accessible R38 roadcut in the Moodies basal conglomerate at Ezzy's Pass, Eureka Syncline, have been dated in six publications (van Niekerk and Burger, 1978; Tegtmeyer and Kröner, 1987; Kröner and Compston, 1988; Sanchez-Garrido and others, 2011; Agangi and others, 2018; Kröner and others, 2018a). We will discuss findings from these studies below.

Most detrital zircon age spectra from Moodies units show four peaks (summaries in Sanchez-Garrido and others, 2011, and Drabon and others, 2017), corresponding to phases of felsic magmatism in the BGB: 1) at *ca.* 3530 Ma (Theespruit and Sandspruit Formations at the base of the Onverwacht Group; Kröner and others, 2016), 2) at *ca.* 3440 Ma (the H6 (rhyo-)dacites of the upper Hooggenoeg Formation, a unit also variably referred to as the Noisy Formation by Grosch and others (2011), the Noisy Complex, or the Buck Ridge Volcanic Complex by de Vries and others (2010); see also Lowe and Byerly, 2020), 3) at *ca.* 3300 to 3280 Ma, corresponding to thin felsic tuffs in the Mendon Formation (Decker and others, 2015), and 4) at *ca.* 3260 to 3220 Ma (shallow intrusive and volcanic rocks in the Auber Villiers, Bien Venue, and Schoongezicht Formations of the upper Fig Tree Group, extending into the Moodies Group; Byerly and others, 1996; Kröner and others, 1991). The oldest

peak is usually, but not always, the smallest peak in frequency histograms and probability density graphs. Zircons >3570 Ma are very rare in the BGB; some of them are found as xenocrysts in younger magmatic rocks (Hoffmann and Kröner, 2018; Moyen and others, 2018). The few other pre-Kaapvaal-aged zircons as old as 3800 Ma and the very rare Hadean zircons documented in the BGB are nearly all from the Green Sandstone Bed of the Mendon Formation (uppermost Onverwacht Group) and are likely impact-related (Drabon and others, 2017; Byerly and others, 2019; Lowe and others, 2021) and derived from outside the BGB.

LA-ICP-MS and SHRIMP ages of *ca.* 3223 to 3219 Ma from pristine tuffs within the Moodies Group were interpreted by Heubeck and others (2013) as representing crystallization during syn-depositional Moodies volcanism and to approximately reflect depositional ages. Virtually all ages from the base to near the top of the unit, a thickness exceeding 3.5 km, overlapped each other within analytical uncertainty. They suggested that Moodies strata were rapidly deposited and offer a high stratigraphic resolution.

SAMPLES

Table 1 shows data from 31 published and unpublished detrital zircon samples from the Moodies Group. Published data sets include those of Tegtmeyer and Kröner (1987), Heubeck and others (2013), Zeh and others (2013), Drabon and others (2017), Stutenbecker and others (2019), Lowe and Byerly (2020), and Reimann and others (2021). Unpublished data sets included in this compilation are from student theses (Luber, ms, 2012; Wiechert, ms, 2014; Leisgang, ms, 2017) and from unpublished data sets of the authors (Byerly, unpublished; Drabon, unpublished; Heubeck, unpublished; Kröner, unpublished). Figure 4 shows the sample locations and table S1 (Supplementary Data) presents the analytical data tables.

The set of 31 samples includes 23 sandstones and seven thin felsic tuffs of which zircon age spectra indicated that they had been aqueously reworked (table 1). These had originally been collected and analyzed to constrain eruption ages, the maximum depositional age or to identify the oldest grain in the sample set. The reworked tuffs are not ideal to characterize proportional age provenance contributions of source rocks because the spectra tend to be heavily biased towards the eruption age and will also be affected by the degree of tidal and fluvial reworking in the braided streams, estuarine deltas, and tidal environments of the Moodies Group. Some or many of these zircons may also represent magmatic xenocrysts.

The final sample represents a compilation of 25 granitoid clasts from the basal conglomerate at Ezzy's Pass, Eureka Syncline. In analyzing these clasts, we treated each clast as representing a single age, even if the clast had yielded multiple single-zircon ages.

METHODS AND ANALYTICAL PROCEDURES

Sample processing and analytical protocols are listed in the Supplementary Data.

Three samples were analyzed by Sensitive High-Resolution Ion Microprobe (SHRIMP: Beijing SHRIMP Center and Stanford University), 28 samples by Laser Ablation – Inductively Coupled Mass Spectroscopy (LA-ICP-MS: Univ. Mainz/Germany; Univ. Frankfurt/Germany; Senckenberg Institution, Dresden/Germany; Univ. of Arizona LaserChron Center, Tucson/AZ, USA; and GEUS Copenhagen/Denmark) (table 1).

The merging of analytical data from seven labs (table 1), each following its own protocol, may be potentially problematic. However, nearly all of the data were acquired post-2010 on modern equipment, and work was performed in labs regularly participating in international calibration surveys using reference material (see

TABLE 1

Moodies Group detrital zircon samples

Within each region, samples are numbered in ascending stratigraphic order where known

No. in Fig. 4	Sample Nr.	Zircons used in prov. analyses	Zircons dated	Location	Stratigraphic position	Latitude	Longitude	Lithology	Reference	Dated by / at	Method	Collected by / field book number of
North of Inyoka Fault												
Eureka Syncline and correlative Moodies Hills Block												
1	BA 121	16	16	Ezzy's Pass	Md basal cgl	25° 41.062'S	31° 9.981'E	sandy conglomerate matrix	Kröner, pers. comm. CH 03/02/2013	Beijing SHRIMP Center	SHRIMP	A. Kröner
2	MdbC	23	25	Ezzy's Pass	Md basal cgl	25° 41.062'S	31° 9.981'E	granitoid conglomerate clasts	Tegtmeyer and Kröner (1987)	Univ. Mainz	LA-ICP-MS	A. Kröner
3	BA 122	17	19	Sheba Road just s of turnoff	basal MdQ, north limb	25° 41.398'S	31° 10.473'E	tidal-facies sandstone	Kröner, pers. comm. CH 03/02/2013	Beijing SHRIMP Center	SHRIMP	A. Kröner
4	MO	183	218	roadside outcrop of tarred rd to Sheba Mine	basal MdQ, north limb	25°41′429″S	31°10′484″E	tidal-facies sandstone	Zeh and others (2013)	A. Zeh, Univ. Frankfurt	LA-ICP-MS	A. Zeh
5	13-379	9	23	Fig Tree Ck. streambed at Old Sheba cementery	basal MdQ, south limb	25° 42.603'S	31° 10.083'E	aquatically reworked tuff	Wiechert (2014)	A. Zeh, Univ. Frankfurt	LA-ICP-MS	C. Heubeck
6	12-071	13	23	lower Clutha Creek	basal MdQ, west limb	25° 42.003'S	31° 4.694'E	tidal-facies sandstone	Leisgang (2017)	Y. Rojas Agramonte, Univ. Mainz	LA-ICP-MS	S. Nabhan
7	MdQ-1	19	21	Moodies Hills Block, Princeton Top	MdQ2	25° 50.240'S	30° 59.442'E	sandstone	Drabon, unpublished	Univ. Arizona LaserChron Center	LA-ICP-MS	N. Drabon
8	12-593	32	95	Eureka City Road, roadside outcrop	top MdS3	25° 43.201'S	31° 5.628'E	aquatically reworked tuff	Heubeck, unpublished	U. Linnemann, Senckenberg Dresden	LA-ICP-MS	C. Heubeck
Total number:		*312*	*440*									

TABLE 1
(continued)

Within each region, samples are numbered in ascending stratigraphic order where known

No. in Fig. 4	Sample Nr.	Zircons used in prov. analyses	Zircons dated	Location	Stratigraphic position	Latitude	Longitude	Lithology	Reference	Dated by / at	Method	Collected by / field book number of
South of Inyoka Fault												
Western BGB, Stolzburg Syncline												
9	12-003-4	17	31	Farm Schoongezicht 713 JT	middle MdQ1	25°53.910' S	30°51.438' E	fluvial, poorly sorted ss	Heubeck, unpublished	Y. Rojas Agramonte, Univ. Mainz	LA-ICP-MS	S. Nabhan
10	11-245	10	104	Farm Belvue 711 JT	MdS1	25.917964° S	30.829233° E	reworked lapilli tuff	Luber (2012)	A. Zeh, Univ. Frankfurt	LA-ICP-MS	T. Luber
11	16-305	55	170	Farm Belvue 711 JT	base MdQ2	25°54'22.00"S	30°49'56.43"E	well sorted high-q ss	Leisgang (2017)	Y. Rojas Agramonte, Univ. Mainz	LA-ICP-MS	C. Heubeck
12	14-044	34	62	Farm Belvue 711 JT	top MdQ2	25°54'35.66"S	30°49'47.96"E	quartzite	Leisgang (2017)	Y. Rojas Agramonte, Univ. Mainz	LA-ICP-MS	C. Heubeck
13	16-303	51	104	Farm Doyershoek 702 JT	top MdQ3	25°54'35.51"S	30°48'57.36"E	well sorted high-q ss	Leisgang (2017)	Y. Rojas Agramonte, Univ. Mainz	LA-ICP-MS	C. Heubeck
Total number:		*167*	*471*									
central BGB, Saddleback Syncline												
14	LS-2012-13	9	24	sw SS, Lomati Delta	MdS1	25°51'51.21"S	31°1'27.55"E	sandstone	Stutenbecker and others (2019)	A. Zeh, Univ. Frankfurt	LA-ICP-MS	L. Stutenbecker
15	2012-15/17/24	65	92	sw SS, Lomati Delta	MdS1	25°51'45.00"S	31° 1'33.02"E	sandstone	Stutenbecker and others (2019)	A. Zeh, Univ. Frankfurt	LA-ICP-MS	L. Stutenbecker
16	NAD-130	110	184	sw SS, Farm Oosterbeek, near R40 road	MdQ	25.842819 S	31.075333 E	sandstone	Drabon and others (2017)	Univ. Arizona LaserChron Center	LA-ICP-MS	N. Drabon
17	09-500	30	36	sw SS	MdS2	25.863215° S	31.007743°	aquatically reworked tuff	Heubeck and others (2013)	A. Zeh, Univ. Frankfurt	LA-ICP-MS	C. Heubeck
Total number:		*214*	*336*									

TABLE 1
(continued)

Within each region, samples are numbered in ascending stratigraphic order where known

No. in Fig. 4	Sample Nr.	Zircons used in prov. analyses	Zircons dated	Location	Stratigraphic position	Latitude	Longitude	Lithology	Reference	Dated by / at	Method	Collected by / field book number of
North of Inyoka Fault												
central BGB, South Africa; near nose of Onv anticline												
18	SA 352-6	9	20	Md Hill in extension of sw THS	Md basal cgl, proximal facies	25° 56.105' S	31° 1.693'E	pebbles and sandstone matrix	Byerly, unpublished	Stanford	SHRIMP	G. Byerly
19	SAF-683-6	122	182	Mzathiya; edge of Dunbar plain at Msauli River	basal Md, proximal facies	25° 59.092' S	31° 01.443'E	sandstone	Lowe and Byerly (2020)	Univ. Arizona LaserChron Center	LA-ICP-MS	G. Byerly
20	PRS-1	102	103	Powerline Road Syncline, south limb	basal Md, ca. 100m above base	25° 53.223' S	31° 0.718'E	sandstone	Drabon, unpublished	Univ. Arizona LaserChron Center	LA-ICP-MS	N. Drabon
21	17-198	24	64	Powerline Road Syncline, north limb	basal Md, ca. 100m above base	25.881219° S	31.012527° E	aquatically reworked tuff	Reimann and others (2021)	T. Thomsen, GEUS Copenhagen	LA-ICP-MS	A. Zametzer
Total number:		*257*	*369*									
central BGB between the Inyoka Fault and the Eswatini border												
22	JAH-663-13	110	111	Paulus's Syncl at R40 roadcut	transitional Fig Tree / Moodies ?	-25.927769°S	31.103856°	sandstone. Fig Tree Gp. ?	Drabon and others (2017)	Univ. Arizona LaserChron Center	LA-ICP-MS	J. Herrington
23	JH05-3	104	123	Paulus's Syncl w of R40 road	transitional Fig Tree / Moodies ?	25.928450° S	31.102567°	sandstone. Fig Tree Gp. ?	Drabon and others (2017)	Univ. Arizona LaserChron Center	LA-ICP-MS	J. Herrington
24	JAH-664-2	163	202	northern Emlembe Access Rd.	basal Moodies ?	-25.923283°S	31.112933°	sandstone	Drabon and others (2017)	Univ. Arizona LaserChron Center	LA-ICP-MS	J. Herrington
25	JH03-1	18	33	northern Emlembe Access Rd.	basal Moodies ?	-25.923683° S	31.109967°	sandstone	Drabon and others (2017)	Univ. Arizona LaserChron Center	LA-ICP-MS	J. Herrington

TABLE 1
(continued)

No. in Fig. 4	Sample Nr.	Zircons used in prov. analyses	Zircons dated	Location	Stratigraphic position	Latitude	Longitude	Lithology	Reference	Dated by / at	Method	Collected by / field book number of
Within each region, samples are numbered in ascending stratigraphic order where known												
North of Inyoka Fault												
central BGB between the Inyoka Fault and the Eswatini border												
26	NAD-128	83	148	The Heights Syncline, hilltop w of Lebombo Overview	low in the Moodies Gp.	-25.887645°S	31.094668°	sandstone	Drabon and others (2017)	Univ. Arizona LaserChron Center	LA-ICP-MS	N. Drabon
27	NAD-129	48	100	Heemstede Syncline, n limb, along Dup Se Pad	middle Moodies Group ?	25.868654°S	31.058586°	sandstone	Drabon and others (2017)	Univ. Arizona LaserChron Center	LA-ICP-MS	N. Drabon
28	15-103	53	110	Masenjane Block, north slope	>1000m above base Md	25° 51.410' S	31° 5.753'	aquatically reworked tuff	Heubeck, unpublished	U. Linnemann, Senckenberg Dresden	LA-ICP-MS	C. Heubeck
Total number:		579	827									
southern BGB, Eswatini												
29	16-226	24	52	Ntaba Mhlope, Piggs Peak - Bulembu Road	basal Md cgl, matrix	25°56'56.37"S	31°11'54.39"E	gravelly sandstone	Heubeck, unpublished	Y. Rojas Agramonte, Univ. Mainz	LA-ICP-MS	C. Heubeck
30	13-351	6	8	Malolotsha Falls viewpoint, Malolotsha NR	within thick quartzite sandstone	26° 6'59.46"S	31° 6'25.03"E	sandstone / metaquartzite	Heubeck, unpublished	Y. Rojas Agramonte, Univ. Mainz	LA-ICP-MS	C. Heubeck
31	13-342	62	85	Malolotsha Syncline	within thick quartzite sandstone	26° 4.786'S	31° 7.369'E	aquatically reworked tuff	Wiechert (2014)	A. Zeh, Univ. Frankfurt	LA-ICP-MS	C. Heubeck
Total number:		92	145									
		1621	2588	Total number of zircons								

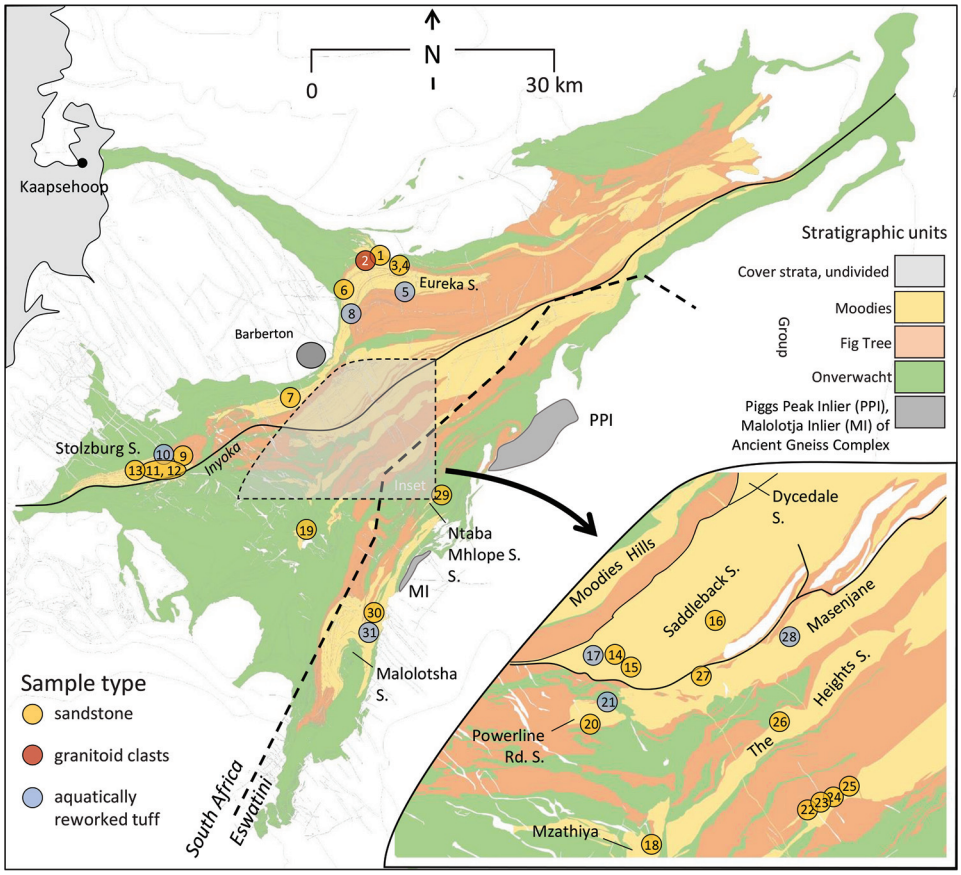

Fig. 4. Geologic map of the Barberton Greenstone Belt showing principal stratigraphic units and locations of samples discussed in the text. See table 1 for locations and stratigraphic information.

Supplementary Data for lab protocols). While the data set is clearly not optimal, the results are internally consistent throughout all datasets, showing very similar age peaks, no lab-based systematic offsets, outliers or other unusual features (fig. 5).

In order to present an all-inclusive "snapshot" of the current data, we decided to include all available data sets of Moodies detrital zircons because the exclusion of smaller data sets of arbitrary minimum size would have introduced an unwarranted selection bias towards larger sample sets and would also have reduced the number of samples available for regional and stratigraphic analysis. The set of 31 samples discussed here is internally consistent and allows regional provenance interpretations. Samples with <30 analyzed zircons passing the quality criteria were treated and plotted along with those having larger numbers. In the histograms and PDF graphs of those data sets, however, peak heights are not conclusive, so that estimates of relative contributions are unreliable, and the absence of peaks may be due to the low numbers of zircons in the sample. In order to balance the number of zircons under consideration in each sample while maintaining accuracy, we adjusted selection ("flag") criteria for degree of concordance, U concentration and 2 sigma standard deviation; see the supplementary data for chosen values. In the 31 data sets, we used 70 to 110, 72 to 104, 72 to 107, and 75 to 110% concordance limits once each, 75 to 106% five times, 80 to 105% once, and in all other data sets >83%. Eleven data sets use limits between

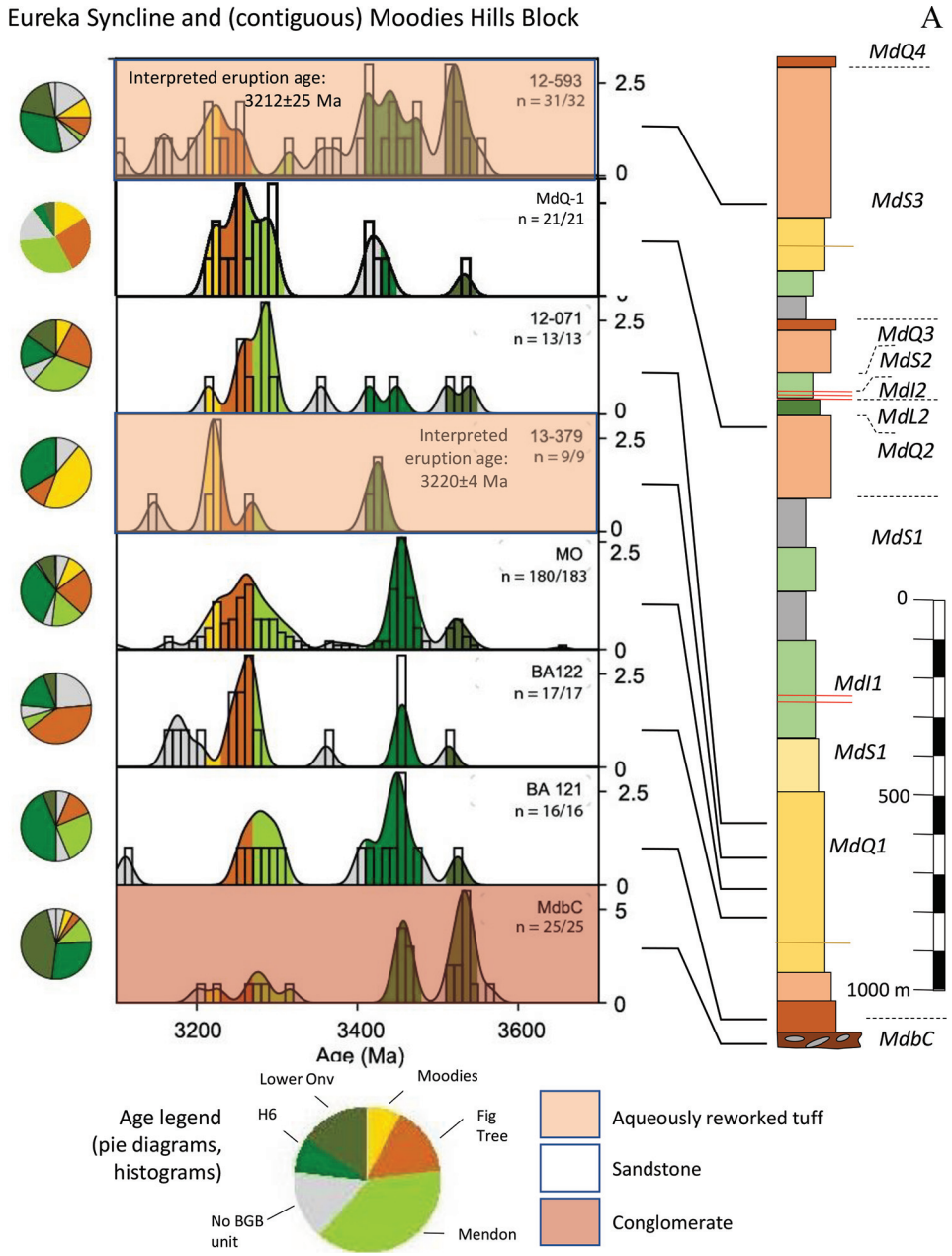

Fig. 5. Frequency histograms and kernel density estimate (KDE) graphs of detrital zircon samples from the Moodies Group. Color scheme in histograms and pie diagrams correspond to ages of major felsic magmatism in the BGB named in the legend. For color scheme of stratigraphic columns, see figure 3. For definition of the regions, see figure 1B. A) Eureka Syncline and contiguous Moodies Hills Block. B) Stolzburg Syncline. C) Saddleback Syncline. D) South of the Inyoka Fault (IF) and close to Onverwacht Anticline. E) Central BGB, south of the IF, north of the South African border. F) South of the Inyoka Fault, Eswatini.

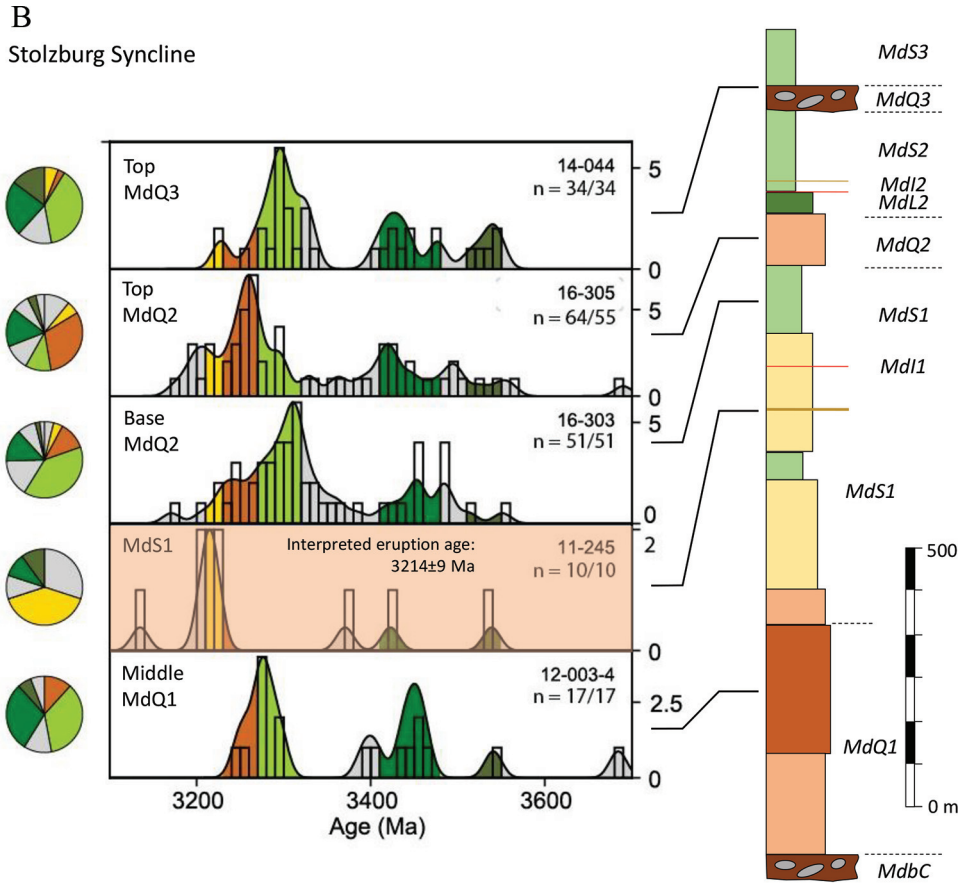

Fig. 5. Continued

90 and 106% concordance. Limits on maximum U concentration range between 380 and 650 µg/g, 2 sigma standard deviations typically at 30 Ma with ranges between 25 Ma and (in two sample sets) 50 Ma. Such an approach is warranted due to the heterogeneous degree of deformation, preservation, post-depositional alteration and degree of metamorphism in the Moodies Group. Data were plotted using DetritalPy, a Python-based toolset for visualizing and analyzing detrital geo-thermochronologic data (Sharman and others, 2018), and IsoPlot 4.15 (Ludwig, 2011).

RESULTS

Complete analytical data are listed in the Supplementary Data, table S1. Detrital zircon age spectra are shown in figure 5.

Sample Characterization

Eureka Syncline (7 samples) and contiguous Moodies Hills Block (1 sample).—We summarized the results from six publications on conglomerate clasts from the Moodies basal conglomerate (MdbC) at Ezzy's Pass in a single detrital zircon spectrum (fig. 5A). Five of the remaining seven data sets sampled the overlying, *ca.* 1000 m thick fluvial- and tidal-facies sandstones (MdQ1, a short-hand term for the stratigraphically first

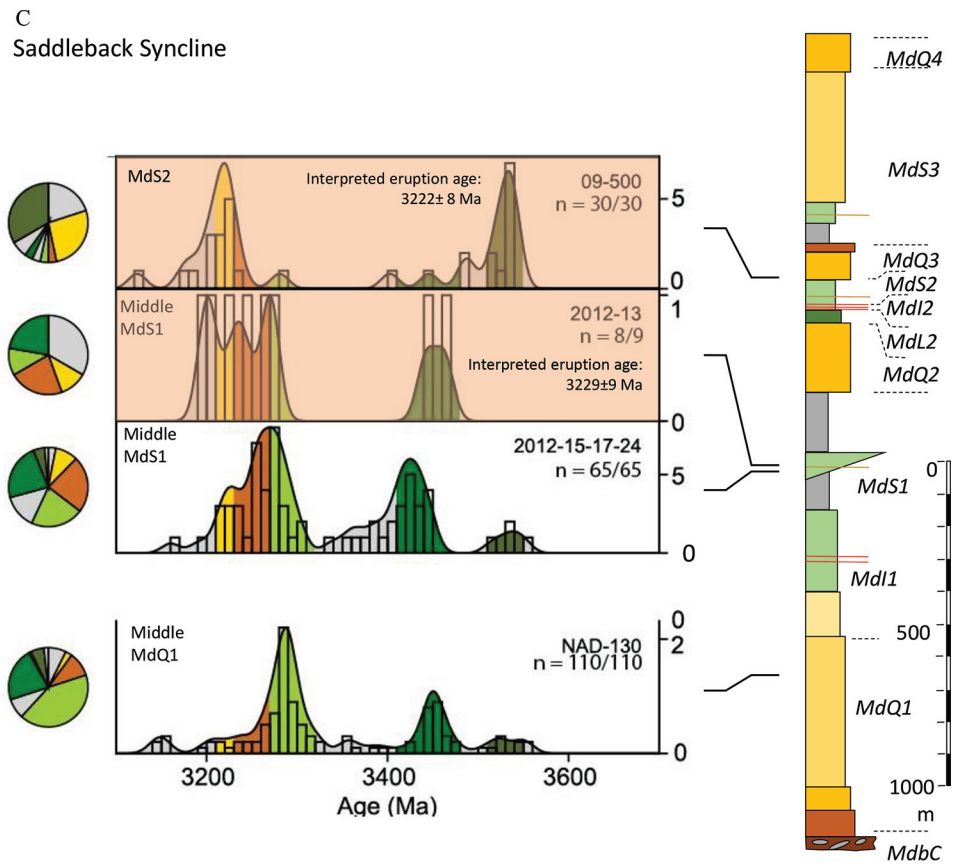

Fig. 5. Continued

"quartzite" in the Moodies Group following the terminology of Anhaeusser (1972), not to be confused with sample MdQ-1). Sample 12-593 represents an aquatically reworked tuff stratigraphically *ca.* 2500 m above base, near the top of the section exposed in the Eureka Syncline (fig. 3). Sample MdQ-1 is from the Moodies Hills Block, structurally and stratigraphically contiguous with the Eureka Syncline but located *ca.* 20 km to the southwest.

Zircon age spectra from all five sandstone samples in figure 5A correspond broadly to the four known peaks of felsic magmatism in the BGB (3550–3530 Ma, 3440–3410 Ma, 3300–3280 Ma, and 3260–3215 Ma) but show differences in detail. The 25 conglomerate clasts of the basal conglomerate MdbC from Ezzy's Pass are dominated by 3.45 and 3.55 Ga zircons (which may be in part due to selective reporting by the original authors). Age spectra of the five samples from the overlying unit MdQ1 are all similar, except for the reworked tuff 13-379, which is dominated by eruption-age zircons. When excluding the basal conglomerate, the proportion of old grains is highest in the stratigraphically uppermost sample 12-593.

The oldest clast of the Moodies basal conglomerate at Ezzy's Pass, clast MD6 in sample MdbC, is 3564.5 ± 2.2 Ma old, based on 19 grains (Kröner and others, 2018a); it confirms the finding from 30 years earlier (Kröner and Compston, 1988). Sanchez-Garrido and others (2011), using a larger zircon database from 16 granitoid clasts, did not find any older zircons. The 3564.5 ± 2.2 Ma age is slightly older than the

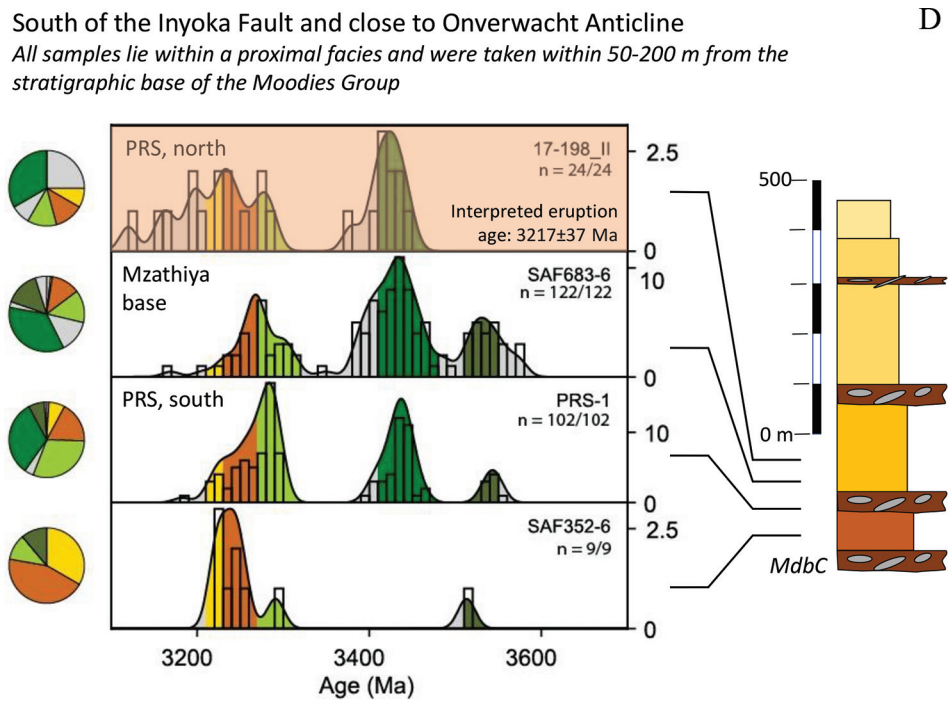

Fig. 5. Continued

oldest zircon crystallization ages from the lowest stratigraphic units of the BGB, felsic volcanic schists of the basal Onverwacht Group near the Steynsdorp Anticline in the southern BGB, which yielded a concordant age of 3552 ± 1 Ma (n = 10; Kröner and others, 2016). That same Moodies conglomerate clast analyzed by Kröner and others (2018a) also contained two xenocrystic zircons with ages of 3602 ± 3 and 3634 ± 3 Ma, approaching the oldest reported age in the Ancient Gneiss Complex (3644 ± 4 Ma; Kröner and others, 1989).

Stolzburg Syncline (5 samples).—Although the Stolzburg Syncline provides one of the best-exposed stratigraphic sequences and was tested by five samples, several samples have low zircon counts which prevents a confident characterization (fig. 5B). The Stolzburg Syncline preserves unusually thick, but poorly exposed, very-fine-grained, rhythmically laminated sandstones and siltstones interpreted as pro-delta facies, punctuated by some delta-front and delta-mouth-bar deposits (Luber, ms, 2012). The aquatically reworked lapilli tuff 11-245 of unit MdS1 shows, as expected, a significant young peak close to its eruption and interpreted depositional age of *ca.* 3214 ± 9 Ma (Heubeck and others, 2013), along with a reduction in the abundance of older grains. The remaining four samples are from deltaic sandstones. They all resemble each other in position and age peaks: Fig Tree provenance dominates, with H6 and lower Onverwacht source rocks subordinate. Sample 16-305 from the base of MdQ2 and sample 12-003-4 from the middle MdQ1 both yielded one grain each >3700 Ma.

Saddleback Syncline (4 samples).—There are only four samples from the large and centrally located Saddleback Syncline (figs. 1A and 5C): two sandstones (NAD-130 and LS 2012-15-17-24) and two reworked tuffs (09-500 and LS 2012-13). The *ca.* 3.5 km-thick stratigraphic sequence in the Saddleback Syncline remains poorly sampled because all but the highest sample are from units MdQ1 and MdS1 in the lower half

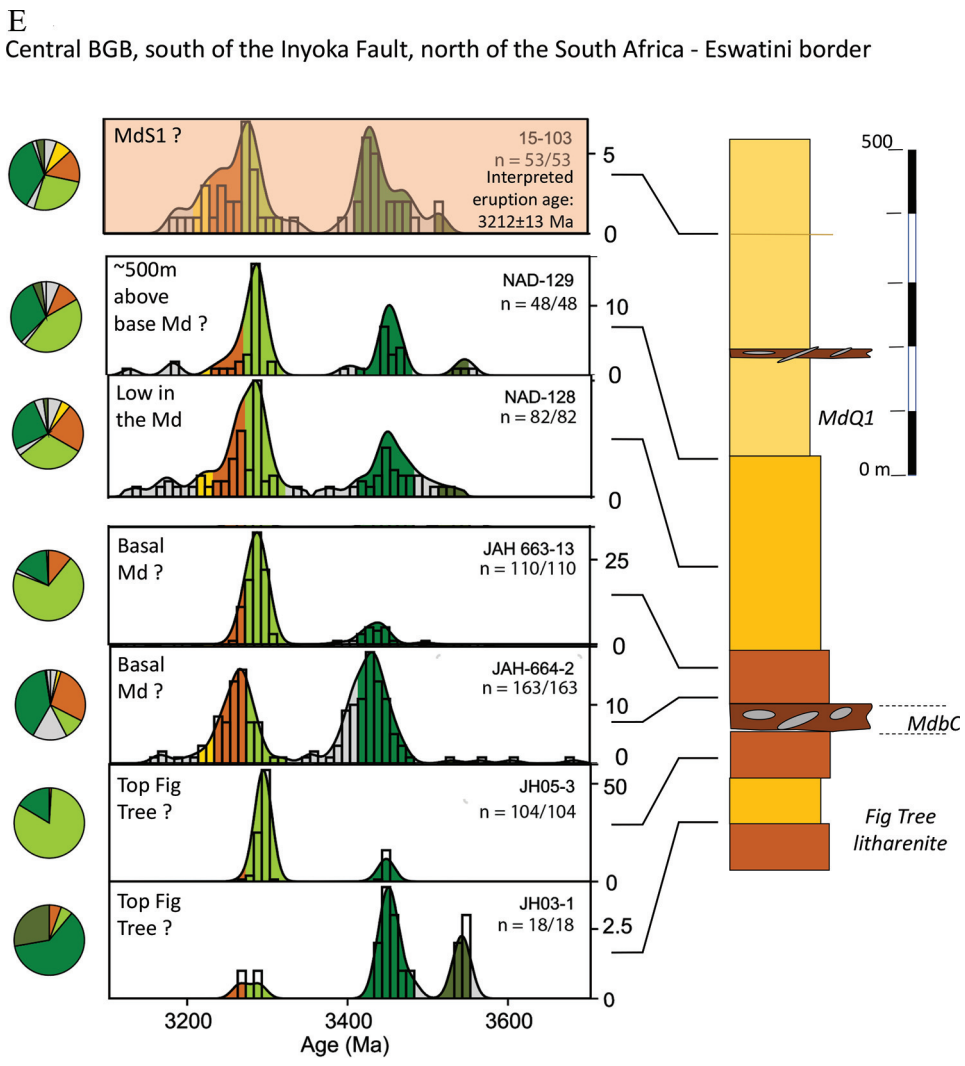

Fig. 5. Continued

of the stratigraphic column. The upper half of the Moodies stratigraphic section, for which depositional environments, sandstone petrography and the presence of intra-formational unconformities attest to a high degree of intra-BGB reworking, has not yet been probed by detrital zircon analyses.

The two sandstone samples NAD-130 and LS2012-15-17-24 strongly resemble each other and both show well-defined peaks (fig. 5C). The former sample represents sheet sandstones in a tidal bar/tidal flat setting. The latter sample is a composite of three sandstone samples from the delta-mouth-bar facies of the Lomati Delta Complex in the southwestern Saddleback Syncline (Stutenbecker and others, 2019). Paleocurrents, bed thickness tapering, grain size and facies changes indicate a clear provenance of these sediments from the region of the Onverwacht Anticline to the southwest (Stutenbecker and others, 2019). Sample LS2012-13 represents a thick bed

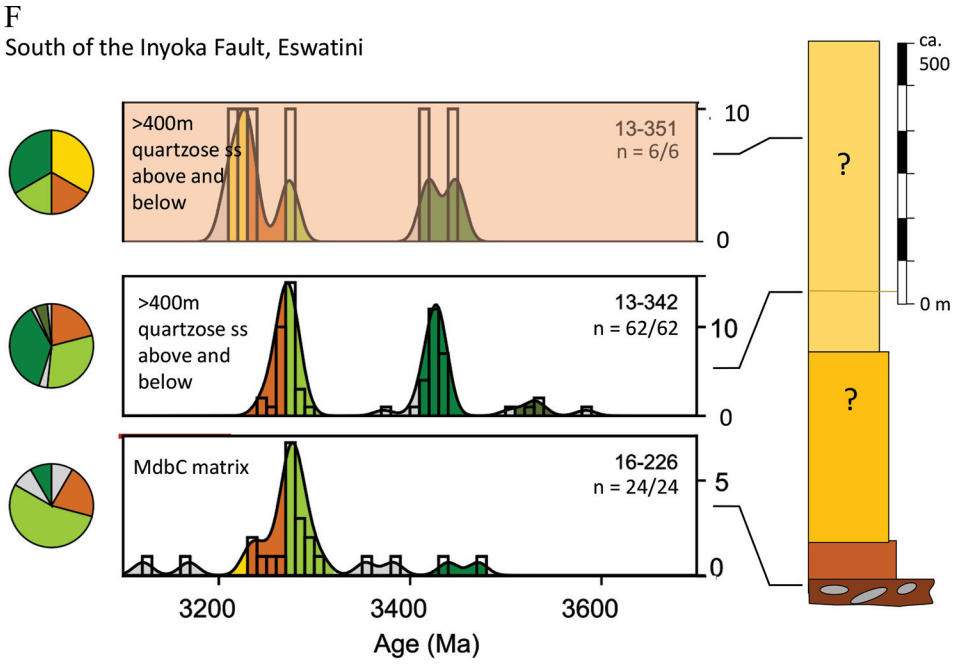

Fig. 5. Continued

of reworked tuffs approximately midway in the Lomati Delta Complex with an age of *ca.* 3229 ± 9 Ma (Stutenbecker and others, 2019). The stratigraphically highest sample, the aquatically reworked tuff 09-500 in a coastal-plain pond setting, shows an unusually high proportion of old (*ca.* 3.54 Ga) grains while also documenting a Moodies-time eruption age with a strong zircon population at *ca.* 3222 ± 4 Ma (Heubeck and others, 2013). It is unclear whether the old grains are magmatic xenocrysts or detrital admixtures.

Central BGB, south of Inyoka Fault; close to Onverwacht Anticline (4 samples).—Three of the four samples originate from medium- to coarse-grained, in places gravelly sandstones exposed in erosional remnants in the central BGB close to the hinge zone of the Onverwacht Anticline (fig. 5D). The stratigraphically highest sample, 17-198, is a reworked tuff, approximately 200 m above the fault-modified base of the Moodies Group in the Powerline Road Syncline, with an imprecise depositional age of 3217 ± 37 Ma (Reimann and others, 2021). While three of the samples show the 3.44 Ga age peak, likely representing contributions from the nearby (rhyo-)dacites of the Hooggenoeg H6 unit, which are widely exposed in the northern Onverwacht Anticline, sample 352-6 from the base of Mzathiya Mountain stands out because of its lack of that age peak. The proximal facies of the host unit to this sample, which comprises interbedded alluvial conglomerates, sandstones and dacitic sills, and the immature composition of the sandstones suggest that this lack of *ca.* 3.44 Ga zircons may be due to a small or geographically restricted drainage basin, located on the margin of the Onverwacht Anticline. However, relationships in this proximal facies belt of the Moodies Group in the central BGB are far from established. They are currently mapped in greater detail in the Powerline Road Syncline (Zametzer, ms, 2019).

Central BGB, south of Inyoka Fault and north of the South Africa – Eswatini border (7 samples).—Moodies strata in the central BGB between the Inyoka Fault and the Eswatini border near Emlembe Mountain are preserved in three SW-NE trending

fault-bounded belts which may be part of a moderately horizontally shortened fold-and-thrust belt (Heubeck and Lowe, 1994; Drabon and others, 2019a; Drabon and Lowe, 2021). In the synclines of this belt, less than 500 m thickness of Moodies strata are estimated to be preserved, but preserved stratigraphic thickness appears to increase towards the NE where the degree of shortening is reduced. Because most Moodies strata in this region are affected by syn- and post-depositional hydrothermal alteration, sandstones of this region are in places recrystallized, silicified, sericitized, and/or fractured (Reimann and others, 2021); as a consequence, Moodies stratigraphy is poorly understood. Sandstone samples JH03-1 and JH05-3 lack Moodies-age zircons (the youngest concordant age clusters are at 3443 ± 4 Ma and 3275 ± 3 Ma, respectively) but carry monocrystalline quartz. They may represent Fig Tree-age strata in an unknown stratigraphic position (compare Drabon and others, 2019b, their fig. 2; Stoll and others, 2021; fig. 5E). The exact depositional setting of the overlying four samples JAH-664-2, JAH663-13, NAD-128 and NAD-129 is uncertain due to poor outcrop and poor accessibility (Stoll and others, 2021). Strata in the The Heights Syncline and along strike of sample NAD-128 are likely to be from tidal-estuarine and coastal-plain facies, based on the nearby presence of microbial mats, mudcracks and ripple planes (Heubeck, unpublished field data). All four samples show similar age spectra in which the oldest peak (*ca.* 3.54 Ga) is poorly developed (fig. 5E). Sample 15-103 is from a discontinuous, aqueously reworked tuff in the Masenjane Block; its zircon age spectrum will be discussed below.

Central and southern BGB, Eswatini (3 samples).—Moodies structure and stratigraphy in Eswatini are currently too poorly understood to allow an interpretation of the three available detrital zircon age spectra (fig. 5F). Lamb (1987) suggested that the onset of Moodies deposition may be diachronous and associated with progressive unconformities in the Malolotsha area. Age spectra from the matrix of the Moodies basal conglomerate in the Ntaba Mhlope Syncline (sample 16-226; sample Nr. 29 in fig. 4; Schmitz and Heubeck, 2021), and from a sandstone sample from the northern Malolotsha Syncline (sample 13-351) show neither unusual proportions nor peak positions. Sample 13-342, an aqueously reworked meta-tuff in the Malolotsha area, lacks young grains and indicates a maximum depositional age as old as 3250 Ma (Wiechert, ms, 2014).

Reworked tuffs.—Of the seven aqueously reworked tuffs in this study, three (samples 12-593 and 13-379 from the Eureka Syncline; sample 15-103 from the Masenjane Block; figs. 4, 5A, E) represent previously unpublished data that contribute to constrain the onset and the end of Moodies deposition. They also illustrate the complexity and uncertainties of chronostratigraphic dating in the Moodies Group and are thus discussed individually below. Table 1 lists sample data, table S1 presents the zircon analytical data.

Sample 12-593 (fig. 6) is a yellowish, fine-grained, sandy dacitic tuff *ca.* 10 cm thick from a roadcut along Eureka City Road in the southwestern Eureka Syncline (figs. 1, 4). The sample location is within cross-bedded, in places gravelly, sandstones with occasional mudcracked shale coats of rippled bedding planes within unit MdS3, close to the core of the Eureka Syncline and thus high in the Moodies stratigraphy. It forms the stratigraphically highest sample from the Moodies Group so far analyzed (unit 10 in fig. 6.11 of Heubeck, 2019, a stratigraphic column along Eureka City Road). Sample 12-593 yielded 95 grains (fig. 6A), of which 43 grains passed the flag criteria 85<conc.<105, U<400 ppm, and 2 sigma <43 Ma. Six, in part nearly concordant grains are distinctly younger than the depositional age (grain a10, at 2950 ± 27 Ma, 65% concordant; grain a18, at 3104 ± 20 Ma, 93% concordant; grain a27, at 3137 ± 30 Ma, 79% concordant; grain a35, at 3036 ± 30 Ma, 106% concordant; grain a48, at 3156 ± 22 Ma, 100% concordant; and grain a56 at 3165 ± 16 Ma, 106%

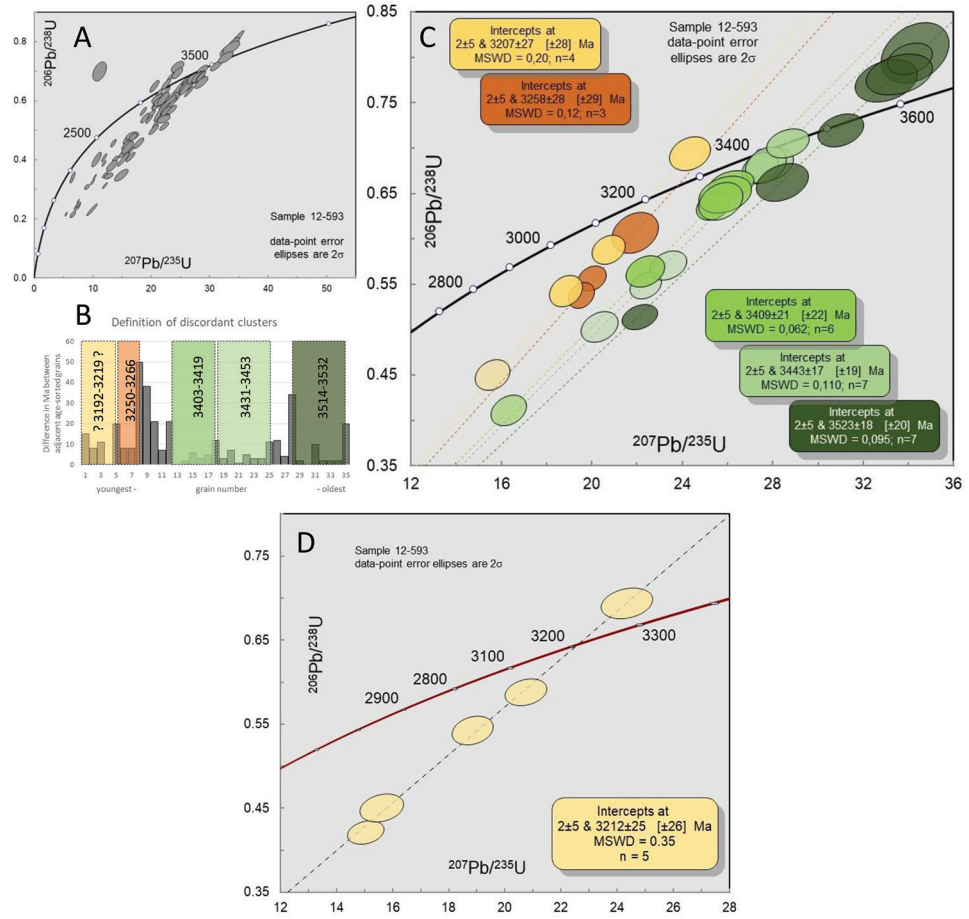

Fig. 6. Concordia diagrams of zircon ages from an aqueously reworked tuff in the Eureka Syncline (sample 12-593, unit MdS3; see fig. 6.11 in Heubeck, 2019, for a stratigraphic column). This is the stratigraphically highest dated bed known in the Moodies Group, constraining end of deposition and timing of syn-sedimentary deformation. A) All 95 zircons; reverse discordance indicates extensive disturbance. B) Histograms of 37 grains which passed the quality test, plotting differences in $^{207}Pb/^{206}Pb$ ages (in Ma) between age-sorted grains. Low values define grains of similar ages. The histogram allows extraction of five clusters with a total of 27 grains. C) Discordia (concordia upper intercept) ages of each cluster correspond to ages of known felsic magmatism in the BGB. D) Discordia from the youngest cluster after adding a 70%-concordant grain that changes the concordia-upper intercept age slightly to 3212±25 Ma, representing the maximum depositional age of this sample. See text for discussion.

concordant) and were eliminated from further consideration; we will discuss their significance below. The remaining 37 age-sorted grains are composed of five clusters defined by similar Pb^{207}/Pb^{206} ages (fig. 6B). These individual populations of three to seven, mostly near-concordant grains were used to calculate individual discordant ages (fig. 6C). Twenty-seven of the 37 grains can be assigned to one of five discordias: 3207 ± 27 Ma (n = 4), 3258 ± 28 Ma (n = 3); 3409 ± 21 Ma (n = 6); 3443 ± 17 Ma (n = 7); and 3523 ± 18 Ma (n = 7). All these correspond to known ages of felsic magmatism in the BGB.

Adding one lower concordant (70% conc.) grain to the discordia of the youngest cluster (n = 5) changes the result slightly to 3212 ± 25 Ma but improves the MSWD (fig. 7D). Adding all available grains in that same young cluster, regardless

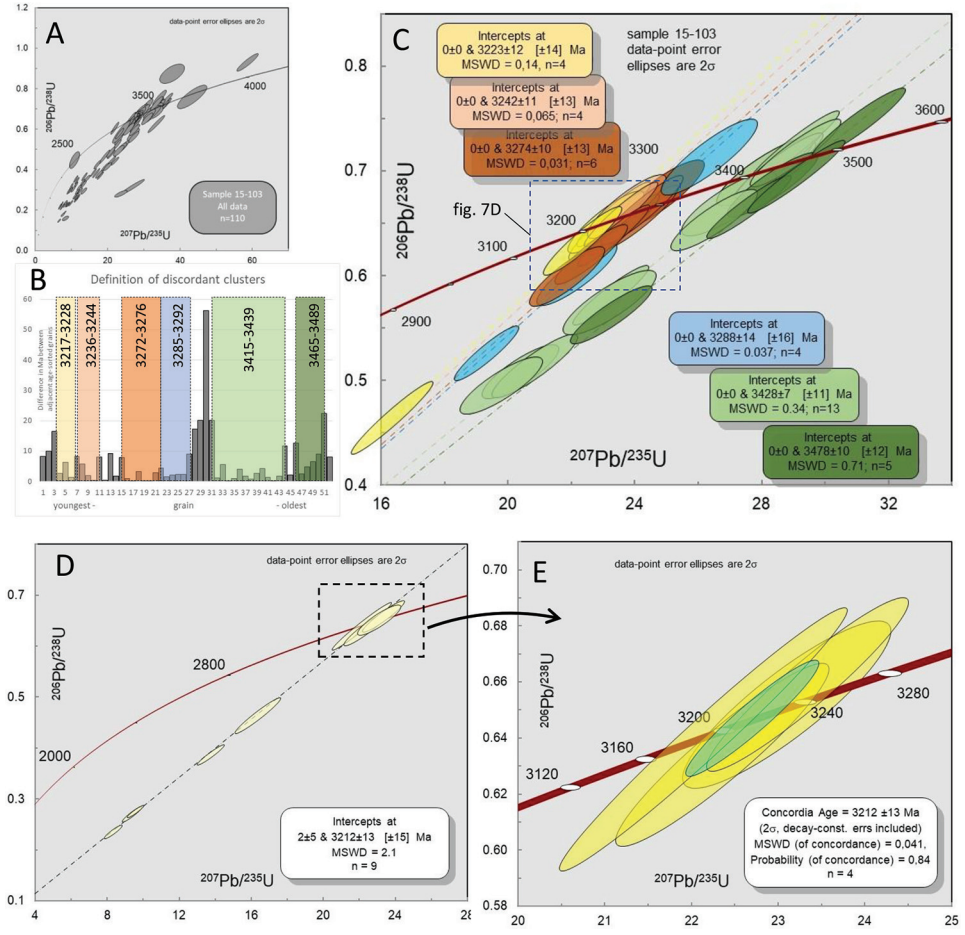

Fig. 7. Concordia diagrams of an aqueously reworked tuff in the Masenjane Block (sample 15-103), a Moodies Group homocline in the central BGB just south of the Inyoka Fault (fig. 3, table 1). The sample is underlain by *ca.* 1000 m of Moodies sandstone. A) All dated zircons (n=110); B) Histogram showing difference in $^{206}Pb/^{207}Pb$ ages (in Ma) of 52 high-quality grains against age-sorted grain number. Low values represent zircons of similar ages, allowing the definition of age clusters for discordia calculations. C) Concordia diagram showing 36 grains conforming to the six discordias, all representing time periods of felsic magmatism in the BGB. The green and light-blue cluster may be identical. D) Youngest discordant cluster, interpreted to represent eruption age and the approximate maximum depositional age of the tuff at 3212±13 Ma; E) Four concordant grains from that cluster yield an identical age of 3212±13 Ma, interpreted as the maximum depositional age of this bed.

of their quality (n = 8), yields an age of 3209 ± 20 Ma but reduces the MSWD (not shown). We conclude that this tuff bed includes a detrital mixture of distinct zircon populations similar to the spectra of detrital zircon samples from Moodies sandstones. The likely maximum depositional age of this bed is approximately 3212 ± 25 Ma.

Sample 15-103 (fig. 7) shows a similar complexity. It was obtained from the Masenjane Block, a structurally complex, probably homoclinal, hydrothermally-altered Moodies unit *ca.* 1000 m thick and intruded by a mafic dike stockwork. The sample is a pale yellow, sandy tuff between thick cross-bedded medium- to coarse-grained sandstones, some with well-preserved shallow-water microbial mats (Homann and others, 2015). Sample 15-103 yielded 110 analyses from as many grains (fig. 7A).

52 grains passed the flag criteria 75<conc.<106%, U<500 ppm, and 2 sigma <50 Ma. Thirty-six of these grains can be assigned to one of six clusters defined by similar Pb^{207}/Pb^{206} ages (fig. 7B). These six populations of four to thirteen, mostly near-concordant grains were then used to calculate individual discordant ages (fig. 7C): 3223 ± 12 Ma (n = 4), 3242 ± 11 Ma (n = 4), 3274 ± 10 Ma (n = 6), 3288 ± 14 Ma (n = 4), 3428 ± 7 Ma (n = 13), and 3478 ± 10 Ma (n = 5). The 3274 ± 10 Ma and 3288 ± 14 Ma clusters overlap (fig. 7C). The youngest discordia cluster, interpreted as representing the maximum depositional age, has an upper-intercept discordia age of 3223 ± 12 Ma (n = 4). This age does not change within error of uncertainty when augmented by four previously-excluded discordant grains of nearly identical $^{207}Pb/^{206}Pb$ ages and (low-quality) 42, 48, 49, and 65% concordance and by a fully concordant grain of 3191 ± 19 Ma, resulting in an upper-intercept discordia age of 3212 ± 13 Ma (n = 9; fig. 7D); four fully concordant grains in that cluster yield an identical age (table S1, fig. 7E).

The discordia ages are not overly dependent on the selection of quality criteria. When grains with similar $^{207}Pb/^{206}Pb$ ratios but lower concordance are included, discordia ages change little. For example, when three grains with concordance between 75 and 60% as well as three concordant grains of 2 sigma > 50 Ma are added to the cluster (n = 13) at 3428±7 Ma, its discordia age remains unchanged at 3428 ± 7 Ma, based on 19 grains. If all grains in that cluster, regardless of their quality, are considered, the calculated age changes to 3435 ± 11 Ma, based on 21 grains. All of these ages are an excellent fit to the age of Hooggenoeg H6 magmatism.

Sample 13-379 (Wiechert, ms, 2014; fig. 8) is from an aqueously reworked tuff bed, filling a *ca.* 10 m wide and 30 cm deep erosional channel within cross-bedded, in places gravelly, sandstones of the basal MdQ1 unit, approximately 25 m above the top of the Moodies basal conglomerate. It was temporarily exposed in the streambed of Fig Tree Creek near the Old Sheba cemetery on the overturned (southern) limb of the Eureka Syncline. Processing the sample yielded only 23 grains (fig. 8A) of which 9 met the quality criteria. Three concordant grains yielded ages of 3428 ± 8 Ma, 3428 ± 7 Ma and 3413 ± 12 Ma. Four, in part moderately discordant (97, 92, 87, and 76% concordant) grains yielded an upper concordia intercept age of 3220 ± 4 Ma (fig. 8B). The two remaining grains were 98% concordant and had ages of 3147 ± 8 Ma and 3269 ± 12 Ma. We interpret the former age to represent a near-complete resetting of the U-Pb system at *ca.* 3150 Ma, discussed in more detail below, and the latter age a detrital zircon grain from the upper Mendon Formation.

We conclude from these calculations that these complex zircon populations were suited for interpretation, even though the tuffaceous host rocks were aqueously reworked, thermally altered, metamorphosed and recently weathered. Moodies Groups andstones therefore undoubtedly also incorporate material from numerous fully reworked and now unrecognizable former tuffs. Zircon populations of reworked tuffs such as those discussed above represent intermediate stages between the populations of pristine tuffs and those of fully epiclastic sandstones. They yield results compatible with the zircon age spectra from both rock types.

DISCUSSION

Post-Depositional Zircon Ages

A total of 428 of the 2588 grains (~16%) in this study record $^{207}Pb/^{206}Pb$ ages between 2600 and 3200 Ma (fig. 9A). Many of these are concordant or near-concordant grains with ages considerably younger than the Moodies depositional age, estimated at *ca.* 3.2 Ga, and record zircon growth or resetting of the U-Pb system postdating Moodies deposition but occurring prior to deposition of the Black Reef

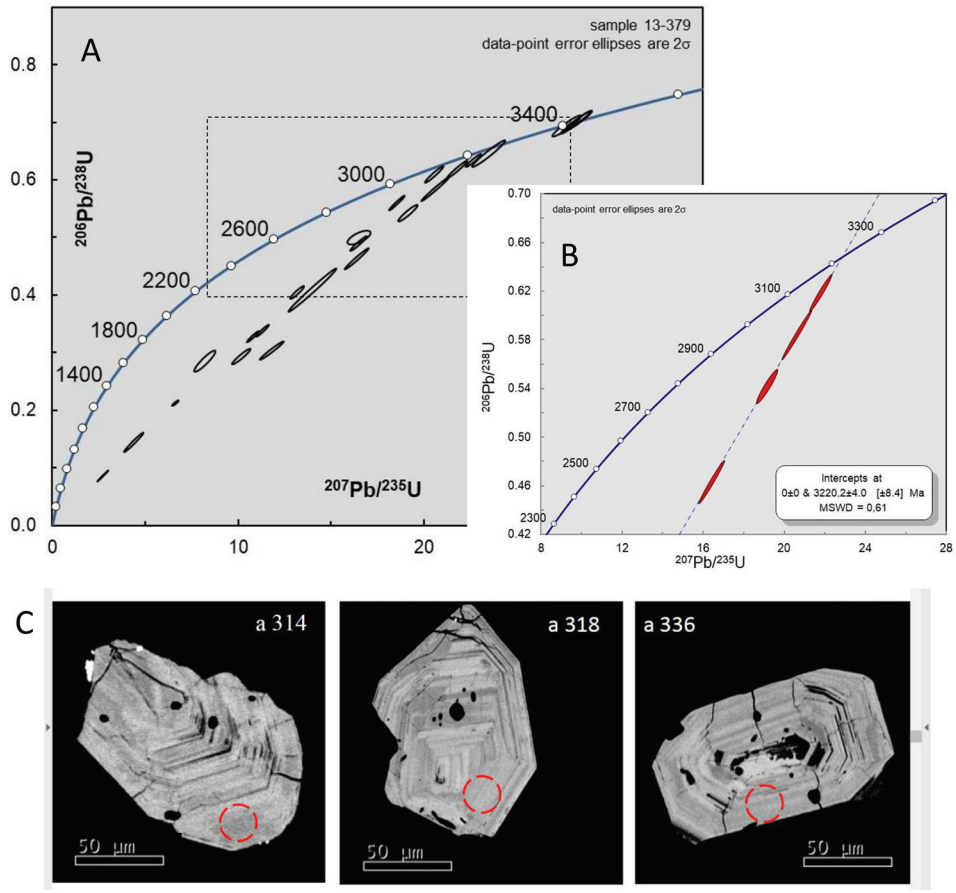

Fig. 8. Age data of sample 13-379, an aqueously reworked tuff filling an erosional channel within gravelly cross-bedded sandstone overlying the Moodies basal conglomerate in the Eureka Syncline (Wiechert, ms, 2014). A) Concordia diagram of all dated grains (n=21); B) Concordia diagram of four grains defining a discordia at 3220±4 Ma; C) Back-scatter-electron (BSE) images of grains a314 (3147±8 Ma, 98% conc.), a 318 (3217±7 Ma, 97% conc.) and a336 (3269±12 Ma, 98% conc). Red dashed circles mark LA-ICP-MS shotpoints. A younger discordia line defines a *ca.* 3150 Ma age, due to a tectonothermal partial reset of the U-Pb system.

Formation at the base of the Transvaal Supergroup at *ca.* 2.6 Ga (Fuchs and others, 2016). Sandstones of this formation unconformably overlie ultramafic volcanic rocks of the Onverwacht Group near the village of Kaapsehoop (fig. 4), *ca.* 30 km northwest of Barberton, and extensively overlie Kaapvaal crystalline basement along the eastern Great Escarpment. Zeh and others (2020) estimate a maximum depositional age of 2618 ± 11 Ma for the Black Reef Formation *ca.* 150 km north of this location. The post-depositional ages in Moodies detrital zircon spectra are best interpreted as reflecting one or several partial or complete resets of the U-Pb system of selected grains by one or several of the hydro- and tectonothermal events which affected the young Kaapvaal craton (Toulkeridis and others, 1998; Olsson and others, 2010; Moyen and others, 2021). A first-order analysis of these 2.6 to 3.2 Ga grains shows a nearly uniform distribution (fig. 9A) but the data set yields better-defined clusters at *ca.* 3.1 and 3.0 Ga as well as possible age concentrations at *ca.* 2.82 and 2.91 Ga when limited to zircons with >80% concordance (fig. 9B). These can be tentatively

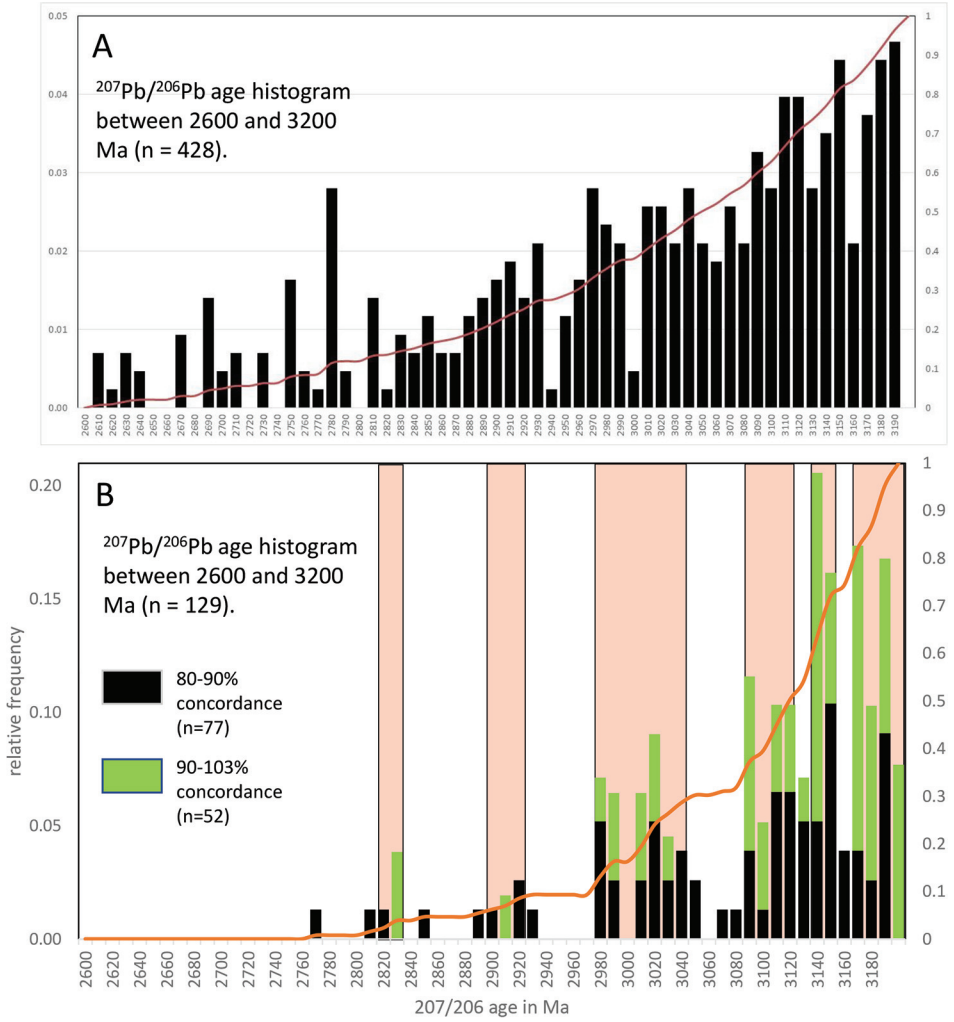

Fig. 9. A. Age histogram of 428 detrital zircons with ages between 2600 and 3200 Ma, not considered in the provenance analysis. The latter had been excluded from provenance analysis in figure 5 due to high U, high standard deviation, or low degree of concordance. No age clustering is recognizable. B. Same data set as above but showing only grains with high concordance (n = 129). The data set appears to host age clusters of *ca.* 2.82, 2.91, 3.0, 3.1, 3.14–3.15, and 3.18 to 3.2 Ga which likely represent tectonothermal events during the early history of the Kaapvaal craton.

related to phases of major magmatic events in the region, such as the voluminous granitic intrusions at 3.0 and 3.1 Ga (see Moyen and others, 2018, for a review; Moyen and others, 2021) and events related to the formation of the Pongola-Mozaan and Witwatersrand basins (for example, Gold and von Veh, 1995; Zeh and others, 2009, 2010). Since 2.6 Ga, and except for (sub-)recent weathering, the U-Pb system in zircons in the region was undisturbed.

Moodies Depositional Age

All detrital zircon data sets examined here are consistent with our previous estimate (Heubeck and others, 2013), based on numerous complementary and consistent

age data, that Moodies deposition north of the Inyoka Fault began at about 3223 ± 1 Ma, experienced syn-depositional deformation at about 3221 ± 1 Ma and ended between 3215 and 3210 Ma (Heubeck and others, 2013) but possibly as early as 3220 Ma. This conforms to the depositional age of 3229 ± 9 Ma proposed by Stutenbecker and others (2019) for the sandstones of the Lomati Delta of unit MdS1 in the Saddleback Syncline. The reworked tuffaceous samples discussed above (samples 13–379, 12-593 and 15-103; figs. 7–9) add the following information: (1) Sample 13–379, *ca.* 100 m above the top of the basal conglomerate in the Eureka Syncline, and with an age of 3220 ± 4 Ma, lies within analytical uncertainty of a previous estimate of the onset of deposition in the Eureka Syncline at *ca.* 3220 ± 4 Ma (Tegtmeyer and Kröner, 1987; Sanchez-Garrido and others, 2011; Zeh and others, 2013; summarized by Heubeck and others, 2013). (2) Deposition in the Eureka Syncline region ended, after more than 3500 m of fluvial, coastal-plain, tidal, and deltaic sediments had been deposited, around 3209 ± 14 Ma (sample 12–593), overlapping within analytical uncertainty with the 3220 ± 4 Ma age of sample 13–379, and suggesting high rates of deposition. (3) The onset of Moodies sedimentation in the central BGB, south of the Inyoka Fault (sample 15-103) and in Eswatini, is poorly constrained because the age of the single sample (16–226) from the base of the Moodies Group in Eswatini is imprecise at *ca.* 3235 ± 15 Ma; stratigraphically higher up, sample 15-103 suggests that sedimentation may have occurred approximately at the same time as north of the Inyoka Fault, at 3208 ± 8 Ma or 3206 ± 11 Ma.

Provenance of Granitoid Clasts from the Basal Conglomerate of the Eureka Syncline

In the absence of a suitable source terrane with ages >3.3 Ga north of the BGB, Kröner and Compston (1988) and Kröner and others (2018a) suspected, based on the old $^{207}Pb/^{206}Pb$ zircon ages in some granitoid clasts of the basal Moodies conglomerate in the Eureka Syncline at the Ezzy's Pass locality, a provenance from the Ancient Gneiss Complex (AGC) to the south. This would point to that region as one of the earliest "continents", that is, a subaerially exposed, eroding region of felsic composition. A southern, but regionally less confined, provenance is also suggested by the εHf_t values obtained from zircons in the oldest conglomerate clast MD6 (Kröner and others, 2018a) and from the single detrital zircon sample in this study analyzed for hafnium isotopes, sample MO (originally published in Zeh and others, 2013). While εHf data from zircons in three Moodies basal conglomerate clasts analyzed by Agangi and others (2018) are ambiguous, εHf values from the sandstone sample MO (Zeh and others, 2013) show a nearly perfect overlap with Hf isotope data obtained from zircons in granitoids (3.2–3.5 Ga age) exposed south of the Inyoka Fault: These zircons include: (1) those from the Stolzburg and Theespruit Plutons which intruded the *ca.* >3.53 Ga Sandspruit and Theespruit Formations at the base of the Onverwacht Group at *ca.* 3.44 Ga in the southwestern BGB and which were partially reactivated at *ca.* 3.23 Ga; (2) those from the *ca.* >3.53 Ga volcanic rocks of these two formations, and; (3) those from the AGC of Eswatini (Zeh and others, 2011; Kröner and others, 2013, 2014a, 2016; Hoffmann and others, 2016; Moyen and others, 2021). Zeh and others (2013; their fig. 5) grouped these magmatic rocks in the "Barberton South Terrane". All these data plot on a crustal evolutionary trend limited by Hf model ages (mantle extraction ages) of 3.5 to 3.75 Ga (two-stage depleted mantle evolution model; Zeh and others, 2009). In contrast, granitoids exposed north of the Inyoka Fault and north of the Barberton Greenstone Belt are characterized by Hf model ages commonly <3.5 Ga (Zeh and others, 2009), making a northern provenance of Moodies detrital zircons difficult, at least for those from the samples analyzed for Hf isotopes. Zircons from the oldest TTGs and grey gneisses in Eswatini (intrusion age >3.5 Ga) indicate derivation from even older depleted mantle sources

between 3.75 and 4.1 Ga (Zeh and others, 2011), which have not been detected so far in detrital zircons in the BGB. The age-Hf isotope signatures from detrital zircons in Moodies sandstone sample MO also overlap with those from nearly coeval metasedimentary (van Schijndel and others, 2017) and metavolcanics rocks (Hoffmann and others, 2020) from the Dwalile greenstone belt and the Kubuta river area (Taylor and others, 2016), both in Eswatini, and may thus identify these regions as potential extra-BGB sources of Moodies sediment. However, the lack of metamorphic conglomerate clasts, of grains of metamorphic provenance (Heubeck and Lowe, 1999; Hessler and Lowe, 2006), of characteristic heavy minerals such as garnet and staurolite in Moodies sandstones, and the facies and thickness pattern of basal Moodies units does not support a provenance from the metamorphic lithologies of the AGC.

Whether sources to the north of the BGB contributed to the Moodies sink is uncertain. Mapping along the northern margin of the BGB, for example in the Eureka Syncline and in the Three Sisters area to the northeast, indicates that the thickness of the Moodies basal conglomerate is highly variable, as is its composition, sorting, and grading, all of which suggest local provenance from lithologically complex sources, rapid mixing of clast types, short transport distance, the reworking of pre-existing gravel, or a combination of some or all of these factors. A short transport distance (and therefore preferably a northerly source; already advocated by Anhaeusser, 1976, 2019) is particularly required for the granitoid clasts which were likely prone to rapid disaggregation under Archean weathering conditions (Hessler and Lowe, 2006). Agangi and others (2018) describe the petrography of three dated clasts in detail: two of them (3522 ± 20 and 3316 ± 10 Ma) are described as porphyritic and possibly volcanic; the third (3286 ± 4 Ma) as probably a shallow intrusive. The common granophyric texture in numerous dated clasts had also been noted as early as 1969 (Anhaeusser, ms, 1969; Sanchez-Garrido and others, 2011). Wang and others (2019) recently dated a sample from the complex Nelspruit Batholith which yielded several ~3.4 Ga zircons. This may hint at the former presence of >3.3 Ga sources north of the BGB, but any potential source rocks there are now incorporated into or covered by the extensive <3.1 Ga granitoids of that region. The lack of a systematic study on the facies, stratigraphy, degree of recycling, and sedimentology of the Moodies basal conglomerate near the Ezzy's Pass location and elsewhere leaves the precise provenance of the 3.5 Ga clasts at that locality currently unresolved (Anhaeusser, 2019).

Source Rocks of the Moodies Group

The provenance interpretation of currently-available Moodies zircon age data suggests that the drainage area(s) of the polymict Moodies basal conglomerate accessed a lithologically varied, highly compartmentalized source area. Stratigraphically higher up, sandstone petrography (Heubeck and Lowe, 1999) and facies analysis (Heubeck and Lowe, 1994; Lowe and others, 2012; Heubeck, 2019) suggest that the Moodies basin became better integrated because sedimentary facies and sandstone petrographic composition converge from their regionally heterogeneous characters. Although sandstone composition becomes highly quartzose, the new source areas apparently did not access rocks of substantially different ages because zircon age peaks do not change substantially up-section but rather continue to overlap with those from intra-BGB rocks, as they did during Fig Tree time (Drabon and others, 2017): They dominantly include feldspar-porphyry volcanic and subvolcanic rocks of the 3.28 to 3.23 Ga Fig Tree Group, the ~3.31 to 3.28 Ga Mendon Formation, the ~3.45 Ga H6 member of the Hooggenoeg Formation, and the 3.51 to 3.54 Ga Sandspruit/Theespruit Formation. Field inspection, petrographic and geochemical analyses of Moodies sandstones and conglomerates also support the erosion of cherts of the Onverwacht Group, the

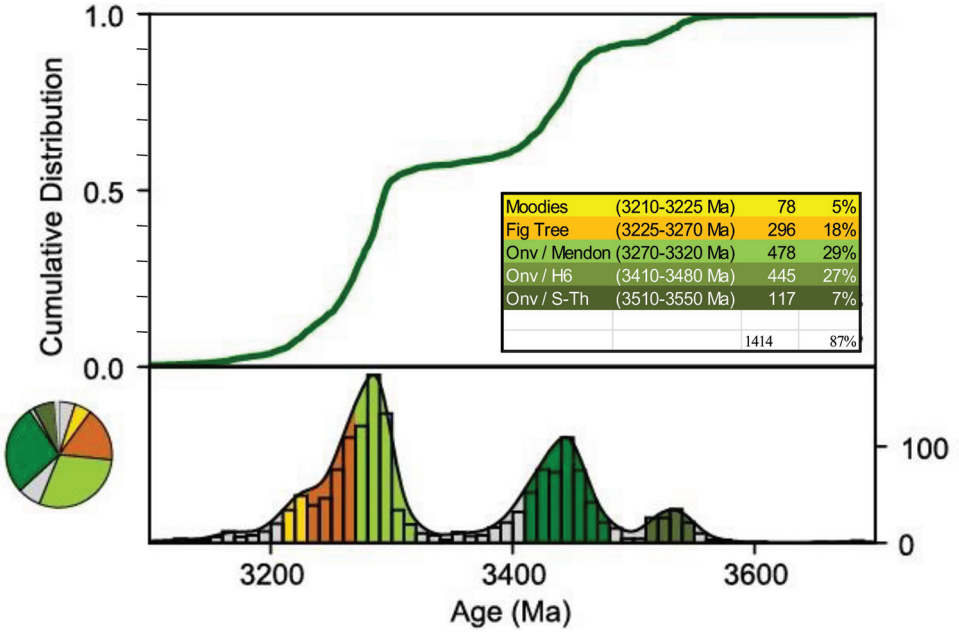

Fig. 10. Summary age distribution graphs of 1621 Moodies detrital zircons from 31 samples which met the quality criteria. Only *ca.* 5% of the population are approximately Moodies age, another 18% approximately Fig Tree age, 63% represent three Onverwacht-age felsic magmatic events. 13% of the zircon population falls outside these five time periods.

recycling of Fig Tree sedimentary rocks, and access to a difficult to quantify, but probably substantial, proportion of ultramafic and mafic volcanic rocks in the source regions (Hessler and Lowe, 2006); they exclude metamorphic rocks. Synoptically, more than two-thirds of Moodies zircons appear to have been ultimately derived from Onverwacht-age rocks (figs. 10, 11), which is also consistent with the composition of conglomerate clasts. Both lines of evidence suggest that Moodies sandstone framework grains may also have been derived in similar proportion from those units of Onverwacht-age lithologies which were suitable for producing sand-sized quartz and microcline.

Our currently-available data for the central BGB, including the match of the detrital zircon age spectra to the ages of potential source rocks, Moodies lithologic and facies pattern, the tectonic position and constraints on timing of uplift, $\delta^{18}O$ data from chert clasts, and εHf isotope data, indicate that a substantial proportion of Moodies sediment was derived in part from the erosion of the Onverwacht Anticline. Whether this region could have been quantitatively capable of sourcing the quartz- and feldspar-rich Moodies sandstones will be explored in the following section.

Relative Contributions by the Fig Tree and Onverwacht Groups

Analysis of detrital zircon age spectra and facies patterns from the Fig Tree Group (Drabon and others, 2017, 2019a; Drabon and Lowe, 2021) shows that Fig Tree strata were, in general, sourced by the older and more mafic strata of the Onverwacht Group. The detrital age spectra from Fig Tree and Moodies sandstones are similar and share evidence for exclusive intra-BGB provenance and a corresponding absence of external sources to the BGB (Drabon and others, 2017; Drabon and Lowe, 2021) even though the tectonic setting of both units may have differed

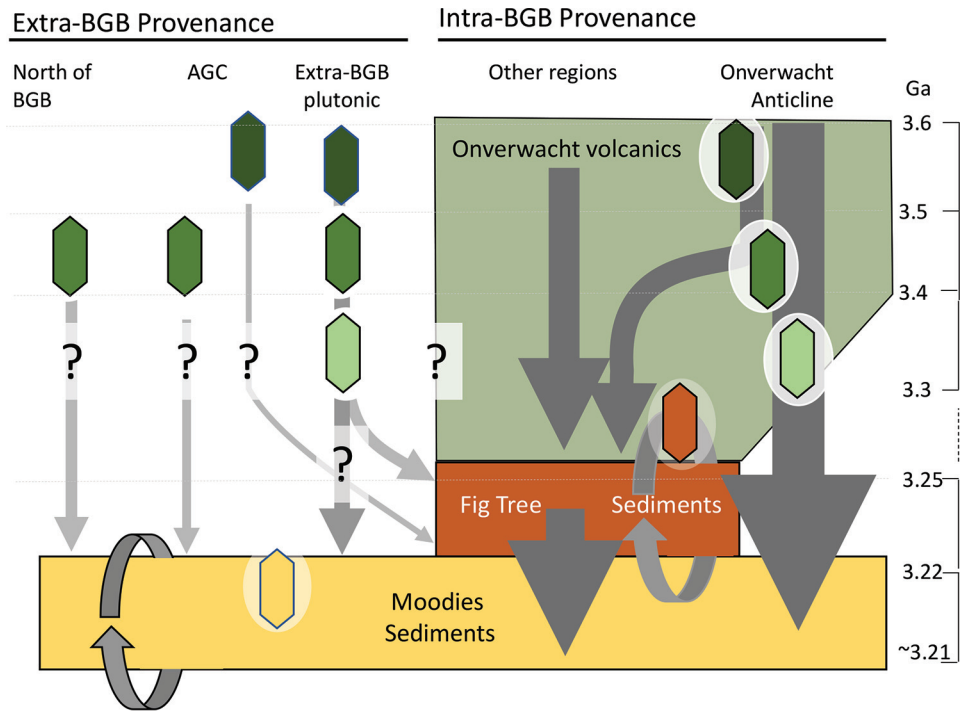

Fig. 11. Schematic provenance diagram showing potential sources of Moodies detrital zircons based on their ages, and also taking into account proximal-distal facies changes in Moodies sediment, εHf isotope values of Moodies detrital zircons and plutons, Moodies sandstone framework petrography, and the potential of BGB stratigraphic units to contribute sand-sized grains to the sandstones of the Moodies Group. Thickness of arrows indicates relative contribution; tone of grey indicates degree of uncertainty (dark = strong evidence). Elliptical arrows indicate intraformational erosion and redeposition (sedimentary recycling). Color scheme as in figure 5.

significantly, and the petrographic mean composition of their sandstones is radically different.

At present, the relative contribution of the Fig Tree Group to Moodies sediments is poorly constrained. The shallow-water, high-energy depositional setting of Moodies Group sandstones efficiently reduced the weathering-prone components of eroded Fig Tree clasts and grains, such as volcanic fragments, shales, tuffs, and intermediate volcanic rocks; in contrast, the same process enriched the more weathering-resistant zircons of Fig Tree provenance (recording Fig Tree and Onverwacht ages) so that they are proportionally over-represented in Moodies detrital-zircon age spectra. In addition, the high degree of sedimentary recycling provided by the tidal regime widespread in Moodies time would have mixed an already complex zircon provenance more efficiently than the deep-water, episodic sedimentation prevalent in the Fig Tree Group. These processes would have driven originally heterogeneous age-provenance sources to greater uniformity in Moodies Group sediments, blurring the original relative contributions from various sources.

Potential Sources External to the BGB

The existence of additional felsic plutonic sources outside the BGB, such as granites (or plutonic bodies of similar composition and considerable size, capable of providing abundant monocrystalline quartz and microcline feldspar), is likely but

difficult to ascertain. Moodies Group sandstones show an impressive and abrupt change in bulk composition compared to Fig Tree sandstones from a mean matrix-rich litharenitic composition of Q47 F4 L49 in Mapepe Formation sandstones (Heinrichs, 1980; Drabon and others, 2019a) with only 4% monocrystalline quartz to a mean approximate Q54 F14 L32 composition in Moodies Group sandstones (Heubeck and Lowe, 1999; Hessler and Lowe, 2006) with >40% monocrystalline quartz. This plausibly demands a shift in provenance and access to new, voluminous, quartz- and feldspar-rich sources (Heubeck and Lowe, 1999; Hessler and Lowe, 2006). The composition and location of these hypothetical source areas is uncertain. Moodies facies patterns in the central BGB indicate a provenance from the Onverwacht Anticline region (the Stolzburg domain of Kisters and others, 2010; see, for example, Lowe and others, 2012) which fits well with evidence for voluminous 3235 to 3225 Ma plutonism, volcanism, metamorphism and uplift in that region (De Ronde and Kamo, 2000; Dziggel and others, 2002, 2005; Kisters and others, 2003, 2010; Lana and others, 2011; Kröner and others, 2018b; Moyen and others, 2018). Uplift and exhumation along the Komati Shear Zone and the Stolzburg Schist Belt is estimated to have occurred at a rate of 1.5 – 5 mm/a (Diener and others, 2005), comparable with estimates of concurrent subsidence rates in the nearby Moodies basin(s) (Heubeck and others, 2013). Because the available εHf data for Moodies Group zircons appear to exclude plutons north of the Inyoka Fault as sources (Zeh and others, 2013), TTG plutons adjacent to the southwestern BGB, namely the Stolzburg (*ca.* 3445 ± 4 Ma) and Theespruit (3443 ± 3 Ma) plutons in the core of the Onverwacht Anticline, the Steynsdorp Pluton (*ca.* 3510 ± 2 Ma), and other smaller plutons, may have acted as possible sources of not only zircons (causing the prominent 3.45 Ga age peak in the histograms; fig. 5) but also of plagioclase, minor microcline feldspar and monocrystalline quartz.

First-order mass balance estimates, however, show that one or several source region(s) larger and richer in monocrystalline quartz than available from the Onverwacht Anticline and adjacent plutons is required to supply the Moodies basin. This contribution is difficult to estimate because the potential of the felsic volcanics in the upper Onverwacht Group, of the aforementioned plutons, and of other now covered or eroded plutons to supply sufficient feldspar and monocrystalline quartz depends not only on their composition and exposed area but also, among others, on topographic relief, intensity of weathering, degree of mineral breakdown during erosion and transport, diagenetic history, mean quartz and feldspar content of Moodies strata, their original thickness, and the original size of the Moodies basin(s). Unfortunately, many of those parameters are virtually unconstrained because both source(s) and sink(s) are only partially preserved and Archean environmental conditions poorly known. Thus, both the degree of delivery of quartz and feldspar from extra-BGB magmatic sources, as well as the volume of quartz and feldspar received by the original Moodies basin(s), remain speculative.

Current evidence therefore appears to indicate that significant extra-BGB plutonic sources with ages similar to those shown by intra-BGB magmatism delivered substantial amounts of monocrystalline quartz and several types of feldspar to the Moodies basin(s). Rapid facies and thickness changes and the presence of thick conglomerates in the southern and northeastern BGB suggest contributions from additional source regions to the Moodies Group, but paleogeographic reconstructions are currently too poor to evaluate the degree of contributions from those regions. The syn-orogenic setting of the Moodies Group, its recognizable facies changes within a few kilometres, and the feldspar content of up to 22% in the Saddleback Syncline (Heubeck and others, 2013), a mineral prone to mechanical abrasion and chemical weathering, appear to require that at least some sources were located close-by; note,

however, that Homann and others (2015) and Reimann and others (2021) argue that the preservation of feldspar and of delicate sedimentary structures were due to very early, near-surface silicification in that region. The currently available zircon age spectra from the Moodies Group thus mostly constrain the age but not the size, type, or location of additional source areas.

Our current understanding of zircon provenance is shown in figure 11. The relative weight of the contributions, symbolized by the thickness of the arrows, not only includes the information from zircon age spectra discussed in this contribution but also considers proximal-distal facies changes in Moodies sediment, εHf isotope values of Moodies detrital zircons and plutons, Moodies sandstone framework petrography, and the potential of BGB stratigraphic units to contribute grains to the sandstones of the Moodies Group.

Stratigraphic Co-Evolution of Age Provenance and Petrography

"Early-Moodies" time, probably within the time period 3223 to 3220 Ma, is widely represented by distal alluvial, in part conglomeratic, and braided fluvial facies, and is lithologically represented by the polymict and laterally heterogeneous Moodies basal conglomerate (MdbC). Up-section, grain size and clast size trends indicate multiple sources; a southwestern provenance, likely from the uplift of the Onverwacht Anticline, appears to be the dominant signal in the central BGB (Knauth and Lowe, 2003; Zametzer, ms, 2019; Heubeck and others, 2020). Subsequently, sedimentation systems became integrated quickly in widespread coastal and tidal plains and in estuarine deltas (MdQ1, MdS1, MdQ2) in which zircon populations show a considerable stratigraphic uniformity.

Knauth and Lowe (2003) documented a stratigraphic up-section trend to lower $\delta^{18}O$ isotope values in Mapepe and Moodies chert clasts, which was inverted from the trend in stratigraphically well-documented cherts from the Onverwacht Anticline. Moodies clasts showed the same low $\delta^{18}O$ values as cherts from the stratigraphically lowest part of that region, perhaps indicating exposure of the Kromberg and Hooggenoeg Formations. Although based on limited samples, Knauth and Lowe (2003) suggested that the inverted isotopic trend observable in the conglomerate chert clasts indicated the stratigraphic "unroofing" of that structure.

Moodies sandstones pass through a marked change in petrographic composition above the Moodies amygdaloidal lava (MdL), a widespread marker unit of andesitic composition and commonly amygdaloidal habit (Heubeck and Lowe, 1999; Heubeck, 2019). While sandstone framework composition below that unit ("mid-Moodies time") shows a gradual increase in monocrystalline quartz concomitant with a gradual decrease in feldspar, polycrystalline quartz grains and chert grains, no large-scale and consistent petrographic trend is currently recognizable above that unit ("late Moodies time"); bed-to-bed changes in petrography are pronounced and appear abrupt, perhaps coinciding with the spotty availability of local sources during folding and shortening of the Moodies basin(s) (the D4 deformation of Byerly and others, 2019). Systematic coverage of the main Moodies stratigraphic sections (of *ca.* 3.5 – 3.7 km thickness each, exposed in the Saddleback and Eureka synclines) by detrital zircon samples, however, is at present too poor to recognize any up-section age trend which could be compared to the petrographic evolution. Perhaps much of Moodies petrographic evolution in "late Moodies" time was dominated by efficient intra-basin recycling which fueled a maturation trend of increasing monocrystalline quartz but did not necessarily change zircon age spectra. Overall, the similarities in zircon age spectra of currently-available Moodies sandstones in the youngest parts of that unit indicate that zircons were largely derived from the same mix of source terranes, but with varying relative contributions from individual sources. Although the stratigraphically

highest samples in the Saddleback, Stolzburg and Eureka synclines (09-500, 14-044, and 12-593, respectively) appear to show a relative enrichment in zircons of the oldest (3.52–3.55 Ga) cohort relative to stratigraphically lower samples, all three samples rely on a small number of zircons; in addition, two of those samples (12-593, 09-500) represent aquatically reworked tuffs and may contain an unquantifiable proportion of magmatic xenocrysts.

CONCLUSIONS

The compilation of 31 detrital zircon data sets from the Moodies Group is internally consistent. They show no conclusive evidence of zircon sources external to the BGB, thus questioning tectonic models that rely on older basement or "hinterland" terranes. In particular, there is no recognizable geochronological evidence of a contribution from the Ancient Gneiss Complex of Eswatini (formerly Swaziland), which is presently in fault contact with the BGB. This agrees with the lack of metamorphic grains and clasts in Moodies Group strata, and with results from facies mapping. Rather, age peaks and sedimentary evidence are consistent with the crystallization ages of zircons in volcanic and plutonic rocks known from the BGB and their role as sources, in part recycling complex zircon populations from those units.

Limited εHf data from the central BGB suggest that predominant zircon sources to the Moodies Group should be located south of the BGB-axial Inyoka Fault. Felsic sedimentary, volcanic and shallow-intrusive rocks eroded from the large, vertically plunging Onverwacht Anticline and TTG plutons intruding its base would meet all those criteria, but are volumetrically insufficient to source Moodies Group quartz and feldspar. Felsic plutonic and subvolcanic sources external to the BGB, now covered or eroded, and with ages corresponding to the documented pulses of BGB magmatism, appear to have been required to supply the large volumes of quartz and feldspar characteristic of the Moodies Group. With the exception of one sample from Eswatini, the youngest coherent cluster of concordant or nearly concordant zircons in all detrital Moodies sandstone samples agrees well with previous estimates of the onset of Moodies deposition around 3223 ± 1 Ma. The end of deposition is less well constrained in this data set, owing to the ambiguous interpretation of aquatically reworked tuffs with complex age distributions. The youngest concordant age cluster of any detrital samples yields an age of 3212 ± 13 Ma, the youngest discordant zircon cluster from the stratigraphically highest sample (an aquatically reworked tuff) yields a discordant age of 3207 ± 27 Ma. Thus, in most BGB regions represented in this data set, top and base of this up to 3.7 km thick shallow-water unit are of nearly identical age within the limits of analytical uncertainty of LA-ICP-MS zircon dating.

ACKNOWLEDGMENTS

CH acknowledges funding through DFG grants He2418/15-1 and He2418/17-1. SAPPI and the Mpumalanga Tourism and Parks agency are thanked for access to land. Frank Linde and Sandra Urban at the Department of Geosciences, Friedrich-Schiller-Universität Jena, expertly processed rocks and prepared thin sections. ND thanks the Arizona LaserChron staff for assistance during data analysis and the Stanford/USGS SHRIMP-RG staff for providing lab space for mount preparation. YRA and AK acknowledge funding through DFG grants KR590/99-1 and RO4174/3-3. Detailed and thoughtful comments by reviewers Carl Anhaeusser, Martin van Kranendonk, Mike Tice and Simon Wilde substantially improved the manuscript.

AUTHOR CONTRIBUTIONS

CH initiated the project, compiled the data, and wrote the main text. ND, YRA, CH, AZ, AK, GB, and DRL sampled in the field, had samples processed, and contributed data sets. ND and CH drew the figures; ND produced detrital age spectra using DetritalPy. ND, DRL, YRA, RMK, and AZ contributed to the text. IL, AGP, YRA, UL, AZ, TBT, RMK and ND performed analyses in the lab and contributed protocols. CH wrote the revised text on which all authors commented.

SUPPLEMENTARY DATA

Table S1: Analytical data

http://earth.eps.yale.edu/%7eajs/SupplementaryData/2022/Heubeck/TableS1Data.xlsx

Table S2: LA-ICPMS operating conditions and data acquisition parameters, GEUS Copenhagen

http://earth.eps.yale.edu/%7eajs/SupplementaryData/2022/Heubeck/TableS2Oper.Parameters_LA-ICPMS_GEUS.pdf

Analytical Procedures

Zircon U-Pb results reported in this study stem from published and unpublished data from seven laboratories listed in table 1. Analyses followed the protocols below.

Mainz University Laboratory (R. Mertz).—Samples 16-303, 16-305, 16-226, 12-003-4, 12-071, 13-351, 14-044 were analyzed and measured by Laser Ablation Inductively Coupled Plasma Mass Spectrometry (LA-ICP-MS) in the Institute of Geosciences, University of Mainz. Approximately 1 to 2 kg of each sample was crushed to a grain size of ~250 μm, using a jaw crusher and roller mill. A heavy mineral fraction (mostly zircon) was obtained by panning with water and ethanol. Zircons for isotopic analysis were handpicked using a binocular microscope (Olympus SZX16) and mounted in epoxy resin and polished to expose their centers. This procedure is needed before imaging the zircons by using an electron microscope (SEM) to obtain cathodoluminescence (CL) images. Imaging with this method delivers insights into the internal structure of zircons such as inclusions, zoning, alteration, fractures, xenocrystic cores and metamict domains. The CL images were used to decide which grains to analyze and where to place the spots.

Zircons were analyzed by using an Agilent 7500ce quadrupole inductively coupled mass spectrometer coupled to an ESI NWR193 ArF excimer laser system with 193 nm wavelength equipped with a TwoVol^2 ablation cell. Ablation was carried out under a He atmosphere with a flow rate of 0.7 L/min and the sample gas was mixed with Ar before entering the plasma. After pre-ablation, analyses were conducted using a 30 μm spot size with 20 s warm up, 30 s ablation and 30 s wash out time. The repetition rate was 10 Hz at energy density of 3.5 J/cm^2, giving a maximum sensitivity. Oxide rates monitored as $^{254}UO/^{238}U$ were below 0.3%. The integration times for individual mass scans were 10 ms for masses 232 and 238, 30 ms for masses 202, 204 and 208. 40 and 60 ms were used for masses 206 and 207, respectively. Reference zircons GJ-1, Plesoviče and 91500 were analyzed after every ten sample zircon spots for calibration and quality control.

Data reduction was performed by using the software PepiAge (Dunkl and others, 2009) to edit the raw data. An in-house Excel^{TM} spreadsheet was used to calculate the different ratios. Time-dependent laser and mass spectrometer-induced inter-element fractionation (Pb/U) as well as mass fractionation and common Pb were corrected

using the same in-house spreadsheet. Where necessary, common Pb was corrected. This included a correction of the interference of ^{204}Hg on ^{204}Pb by measuring ^{202}Hg and using a ^{202}Hg/^{204}Hg ratio of 0.2299 applied to the background-corrected signals at m/z 204 and a model Pb isotope composition (Stacey and Kramers, 1975).

Ages, uncertainties and concordia diagrams were calculated using the Isoplot3 add-in for Excel™ (Ludwig, 2003). Concordia ages were plotted with 2σ error ellipses, and discordia intercept ages are given at 95% confidence. Analyses were calibrated using the 91500 zircon (Wiedenbeck and others, 1995). The reproducibility was controlled by measuring the reference zircons GJ-1 zircon (Jackson and others, 2004) and Plesoviče (Sláma and others, 2008). The results are presented in table S1 where the isotopic ratios are given with 1σ uncertainties. For ages younger than 1.0 Ga, ^{206}Pb/^{238}U ratios were used for interpretation, for ages above 1.0 Ga ^{207}Pb/^{206}Pb was used.

Arizona LaserGeochron Center (N. Drabon).— ^{207}Pb/^{206}Pb ages of samples MdQ-1, NAD-130, SAF-683-6, PRS-1, JAH-663-13, JH05-3, JAH-664-2, JH03-1, NAD-128, NAD-129 were measured by Laser-Ablation Inductively Coupled Plasma Mass Spectrometry (LA-ICP-MS) with a 20 μm spot diameter at the Arizona LaserChron Center using the techniques discussed in Gehrels and others (2008) and Gehrels and Pecha (2014).

Beijing SHRIMP Center (A. Kröner).—Zircon isotopic analyses of Sample BA 121, BA 122 were performed on a SHRIMP II sensitive high-resolution ion-microprobe in the Beijing SHRIMP Center. Analytical procedures are detailed in Kröner and others (2014b) and references therein. The reduced ^{206}Pb/^{238}U ratios were normalized to 0.09100, which is equivalent to the adopted age of 561.3 Ma for reference zircon M257 (Nasdala and others, 2008). For data collection, five scans through the critical mass range were made. Primary beam intensity was between 3.2 and 3.5 nA, and a Köhler aperture of 100 μm diameter was used, giving a slightly elliptical spot size of about 25 μm. Peak resolution at 1% peak height was 4970, enabling clear separation of the ^{208}Pb-peak from the HfO peak. Sensitivity was between 20 and 25 cps/ppm/nA Pb on the reference zircon. Analyses of samples and reference materials were alternated to allow assessment of Pb+/U+ discrimination. The one-sigma uncertainty of the ^{206}Pb/^{238}U ratio during analysis of ten reference zircons during this study was 0.7%. Raw data reduction and uncertainty assessment followed the method described by Nelson (1997), using the Macintosh software programs Prawn 6.4, WALLEAD 2.7 and Plonk 4.3. Common-Pb corrections were applied using the ^{204}Pb-correction method, and because of very low counts on ^{204}Pb in most samples it was assumed that common lead was surface-related (Kinny, 1986). Therefore, the isotopic composition of Broken Hill lead was used for correction. Analyses with ^{204}Pb counts more than three times background were corrected using the Cumming and Richards (1975) values. Uncertainties of individual analyses in table S1 are given at the one-sigma level and are based on counting statistics. They include the uncertainty in the U/Pb age of the reference zircon, added in quadrature (Nelson, 1997). The uncertainty of the pooled analyses is reported at the two-sigma confidence interval. In addition, we checked on instrumental mass fractionation of the SHRIMP II instrument by analyzing seven grains of reference zircon OG-1 during the course of this study. The recommended ^{207}Pb/^{206}Pb ratio and age for this reference zircon are 0.29907 ± 11 and 3465.4 ± 0.6 Ma, respectively (Stern and others, 2009). Our analyses yielded a weighted mean ^{207}Pb/^{206}Pb ratio and age of 0.29912 ± 41 and 3465.7 ± 2.1 Ma, respectively, indistinguishable from the recommended values.

Frankfurt University Laboratory (A. Zeh).—Uranium, thorium and lead isotopes of the samples MO, 13-379, 11-245, LS-2012-13, LS 2012-15/17/24, 09-500, 13-342 were analyzed using a Thermo-Fisher Scientific Element 2 sector field ICP-MS coupled to a Resolution M-50 (Resonetics) 193 nm ArF excimer laser (ComPexPro 102F,

Coherent) system at Goethe-University, Frankfurt, following the method describe in Gerdes and Zeh (2006, 2009). Data were acquired with a 20 second background measurement followed by 21 second sample ablation. Laser spot-size was 33 μm for unknowns and the reference zircons GJ-1 (calibration material), Plesoviče and OG1. Ablation was performed in a He stream, which was mixed directly after the ablation cell with N_2 and Ar prior to introduction into the Ar plasma of the SF-ICP-MS. Signal was tuned for maximum sensitivity for Pb and U, while keeping oxide production, monitored as $^{254}UO/^{238}U$, below 0.5%. The sensitivity achieved was in the range of 9000 to 14000 cps/μg g^{-1} for ^{238}U with a 33 μm spot size, at 5.5 Hz and about 3.5 J cm^{-2} laser energy. The typical penetration depth was about 15 μm. Raw data were corrected offline for background signal, common Pb, laser induced elemental fractionation, instrumental mass discrimination, and time-dependent elemental fractionation of Pb/U using an in-house MS Excel© spreadsheet program (Gerdes and Zeh, 2006, 2009). A common-Pb correction based on the interference- and background-corrected ^{204}Pb signal and a model Pb composition (Stacey and Kramers, 1975) was carried out. For the analyzed samples the calculated common ^{206}Pb contents was mostly <0.5% of the total ^{206}Pb but in rare cases exceeded 2%. Laser-induced elemental fractionation and instrumental mass discrimination were corrected by normalization to the reference zircon GJ-1 (Jackson and others, 2004) as well as inter-elemental fractionation ($^{206}Pb^*/^{238}U$) during the sample ablation. Reported uncertainties (2σ) of the ratio were propagated by quadratic addition of the external reproducibility (2 SD) obtained from the reference zircon GJ-1 and the within-run precision of each analysis (2 SE; standard error).

For $^{207}Pb/^{206}Pb$, we used a ^{207}Pb signal-dependent uncertainty propagation (Gerdes and Zeh, 2009). The $^{207}Pb/^{235}U$ ratio is derived from the normalized and uncertainty-propagated $^{207}Pb/^{206}Pb^*$ and $^{206}Pb^*/^{238}U$ ratios, assuming a $^{238}U/^{235}U$ natural abundance ratio of 137.88 and the uncertainty derived by quadratic addition of the propagated uncertainties of both ratios. Analytical results are presented in table S1. The accuracy of the method was verified during the different sessions by analyses of three reference zircons: GJ-1 (primary standard), Plesoviče and OG1 (secondary standards). Concordia ages obtained from all three reference zircons were always within uncertainty identical to the quoted TIMS values of 337 ± 0.37 Ma for Plesoviče (Sláma and others, 2008), 3465.4 ± 0.6 Ma for OG1 (Stern and others, 2009), and 604.1 ± 0.8 Ma for GJ-1 (in-house value, Goethe-Universität Frankfurt, in agreement with the values quoted in Jackson and others, 2004).

GEUS Copenhagen (T.B. Thomsen).— U-Pb zircon geochronology on sample 17-198 was carried out on mineral separates embedded in epoxy mounts by laser ablation SF ICPMS at the Geological Survey of Denmark and Greenland. A NWR213 solid state Nd:YAG laser system from Elemental Scientific Lasers (ESL) mounted with a standard TV2 ablation cell was coupled to an Thermo-Fisher Scientific Element 2 double-focusing single-collector magnetic sector-field ICPMS. The mass spectrometer was equipped with Ni cones, quartz torch shielded with a grounded Pt electrode and a quartz bonnet. Operating conditions and data acquisition parameters are listed in table S2. The laser was fired for 15 minutes before operation, providing stable laser output energy and flat ablation craters by the "resonator-flat" laser beam. Prior to loading, samples and standards were carefully cleaned using ethanol and an ultrasonic bath to remove surface contamination. The ablation cell with the inserted sample holder was flushed with helium gas to minimize and stabilize the gas blank level. Helium was used as the carrier gas and was mixed with argon gas *ca.* 0.5 m before entering the mass spectrometer. The mass spectrometer was run for at least one hour before analysis to stabilize the background signal.

Just before analysis commenced, the ICP-MS was optimised for dry plasma conditions through continuous linear ablation of the GJ-1 zircon standard. The signal-to-noise ratios for the heavy mass range of interest (that is, ^{202}Hg to ^{238}U), emphasizing ^{238}U and ^{206}Pb, were maximized, while simultaneously opting for low element-oxide production levels by minimising the $^{254}UO_2/^{238}U$ ratio. To minimize instrumental drift, a standard-sample-standard analysis protocol was followed, bracketing 8 zircon analyses by at least six GJ-1 zircon standard measurements. For quality control of the standard analyses, the Harvard 91500 (Wiedenbeck and others, 1995, 2004) and Plesoviče (Sláma and others, 2008) reference zircons were measured regularly during the analysis sequences, both yielding an averaged age accuracy with < 3 to 4% deviation from reference values, and an averaged internal uncertainty of $< 3\%$. Data were obtained from single spot analysis using a laser spot size of 20 μm, a nominal laser fluence of ~9.5 J/cm^2, and a pulse rate of 5 Hz. Acquisition for single zircon analysis included 30 sec. background measurement followed by laser ablation for 30 sec., and washout for 30 sec. Factory-supplied software was employed for the acquisition of the transient data, acquired through automated running mode of pre-set analytical locations. Based on the CL and optical images, analyses spots on the grains were set at inclusion-free locations free of cracks. Data processing and calculation of isotopic ratios and ages were carried out off-line through the software Iolite v. 2.5 (Hellstrom and others, 2008; Paton and others, 2011), using the Iolite-integral VizualAge data reduction scheme by Petrus and Kamber (2012). The VizualAge data reduction scheme includes a correction routine for down-hole isotopic fractionation (Paton and others, 2010) and provides routines for data that require correction for common Pb.

Senckenberg Naturhistorische Sammlungen Dresden (U. Linnemann).—Zircon concentrates of samples 12-593 and 15-103 were separated from *ca.* 2 kg-sized samples at the Department of Geosciences, Friedrich-Schiller University Jena. Samples were crushed in a jaw crusher (Retsch) and sieved by a sieving machine (Retsch). The fraction of 400 to 40 μm was used for heavy mineral separation by making use of heavy liquid (LST, lithium heteropolytungstate), which had a density of 2.85 g/cm^3. Sample powder and heavy liquid was mixed in a separatory funnel. After about one hour, heavy minerals were separated, washed with distilled water, and dried in a drying cabinet at a temperature of 50°C. Final selection of the zircon grains for U–Pb dating was achieved by hand-picking under a binocular microscope. Zircon grains of all sizes and morphological types were selected, mounted in resin blocks and polished to half their thickness.

Zircons were analyzed for U, Th, and Pb isotopes by LA ICP-MS techniques at the Museum für Mineralogie und Geologie (GeoPlasma Lab, Senckenberg Naturhistorische Sammlungen, Dresden), using a Thermo-Scientific Element 2 XR sector field ICP-MS (single-collector) coupled to a RESOlution 193nm excimer laser. Each analysis consisted of approximately 15 s background acquisition followed by 30 s data acquisition, using a laser spot-size of 25 and 35μm, respectively. A common-Pb correction based on the interference- and background-corrected ^{204}Pb signal and a model Pb composition (Stacey and Kramers, 1975) was carried out if necessary. The necessity of the correction was judged on whether the corrected $^{207}Pb/^{206}Pb$ lay outside of the internal errors of the measured ratios (Frei and Gerdes, 2009). Discordant analyses were generally interpreted with care. Raw data were corrected for background signal, common Pb, laser-induced elemental fractionation, instrumental mass discrimination, and time-dependant elemental fractionation of Pb/Th and Pb/U using an Excel® spreadsheet program developed by Albert Richard Roper and Axel Gerdes (FIERCE, Institute of Geosciences, Johann Wolfgang Goethe-University Frankfurt, Frankfurt am Main, Germany). Reported uncertainties were propagated by quadratic addition of the external reproducibility obtained from the standard zircon

GJ-1 (~0.6% and 0.5–1% for the $^{207}Pb/^{206}Pb$ and $^{206}Pb/^{238}U$ ratios, respectively; Jackson and others, 2004) during individual analytical sessions and within-run precision of each analysis. In order to test the accuracy of the measurements and data reduction, we included the Plesoviče zircon as a secondary standard in our analyses which gave reproducible ages of *ca.* 337 Ma, fitting the results of Sláma and others (2008). For further details on analytical protocol and data processing see Gerdes and Zeh (2006). U and Pb content and Th/U ratio were calculated relative to the GJ-1 zircon standard and are accurate to approximately 10%.

Stanford SHRIMP (G. Byerly).— Sample SA352-6: Methodology for extraction, imaging and analysis of zircons follows those of Byerly and others (2018). Analyses were performed using an O_2^- primary ion beam with an intensity varying from 2.8 to 3.0 nA. The primary ion beam spot had a diameter between 20 and 23 microns and a depth of ~2 microns. The acquisition routine included analysis of $^{90}Zr_2{}^{16}O^+$, $^{180}Hf^{16}O^+$, $^{204}Pb^+$, a background measured at 0.045 mass units above the $^{204}Pb^+$ peak, $^{206}Pb^+$, $^{207}Pb^+$, $^{208}Pb^+$, $^{238}U^+$, $^{232}Th^{16}O^+$, and $^{238}U^{16}O^+$. All peaks were measured on a single EPT® discrete-dynode electron multiplier operated in pulse counting mode, with 7 scans (peak-hopping cycles from mass 195.8 through 254). Measurements were performed at mass resolutions of M/DM = 6,500 (10% peak height), which fully separates Pb isotopes from interfering molecular species.

Calculated $^{206}Pb/^{238}U$ model ages for zircon were standardized relative to AS3 (1096 Ma; Paces and Miller, 1993; Schmitz and others, 2003), which was analyzed repeatedly throughout the analytical session. Due to the old ages of the samples, measuring $^{207}Pb/^{206}Pb$ was the main focus of this study, whereas the U/Pb ages were measured only to evaluate concordance (or lack thereof). Measured $^{207}Pb/^{206}Pb$ for unknowns and standards were corrected for instrument mass fractionation by a factor of 0.9957 ± 0.0023 (or decreased by 0.433%) based on calculated weighted mean of $^{207}Pb/^{206}Pb$ measurements for OG1 zircon (3465.4 ± 0.6 Ma; Stern and others, 2009). Data reduction for geochronology follows the methods described by Williams (1997) and Ireland and Williams (2003), and using the Microsoft Excel add-in programs Squid 2.51 and Isoplot 3.764 by Ludwig (2009, 2012). The measured $^{206}Pb/^{238}U$ and $^{207}Pb/^{206}Pb$ values were corrected for common Pb using ^{204}Pb, assuming the model Pb composition of Stacey and Kramers (1975). Zircon concentrations for Hf, U, and Th were standardized relative to the 91500 zircon standard (81.3 ppm U, 28.6 ppm Th, 6030 ppm Hf; Wiedenbeck and others, 1995; Gehrels and others, 2008), which was mounted on a separate setup mount.

REFERENCES

Agangi, A., Hofmann, A., and Elburg, M. A., 2018, A review of Palaeoarchaean felsic volcanism in the eastern Kaapvaal craton: Linking plutonic and volcanic records: Geoscience Frontiers, v. 9, n. 3, p. 667–688, https://doi.org/10.1016/j.gsf.2017.08.003

Anhaeusser, C. R., ms, 1969, The stratigraphy, structure, and gold mineralization of the Jamestown and Sheba Hills areas of the Barberton Mountain Land: Ph.D. thesis, University of the Witwatersrand, Johannesburg, South Africa, p. 332

——, 1972, The geology of the Jamestown Hills area of the Barberton Mountain Land, South Africa: Transactions of the Geological Society of South Africa, v. 75, n. 3, p. 225–263

——, 1976, The geology of the Sheba Hills area of the Barberton Mountain Land, South Africa, with particular reference to the Eureka Syncline: Transactions of the Geological Society of South Africa v. 79, p. 253–280

——, 2019, The geology and tectonic evolution of the northwest part of the Barberton Greenstone Belt, South Africa: A review: South African Journal of Geology, v. 122, n. 4, p. 421–454, https://doi.org/10.25131/sajg.122.0033

Arndt, N. T., and Nesbit, E. G., 2012, Processes on the Young Earth and the Habitats of Early Life: Annual Reviews of Earth and Planetary Sciences, v. 40, p. 521–549, https://doi.org/10.1146/annurev-earth-042711-105316

Bedard, J. H., 2018, Stagnant lids and mantle overturns: Implications for Archaean tectonics, magma genesis, crustal growth, mantle evolution, and the start of plate tectonics. Geoscience Frontiers, v. 9, n. 1, p. 19–49, https://doi.org/10.1016/j.gsf.2017.01.005

Byerly, B. L., Lowe, D. R., Drabon, N., Coble, M. A., Burns, D. H., and Byerly, G. R., 2018. Hadean zircon from a 3.3 Ga sandstone, Barberton greenstone belt, South Africa: Geology, v. 46, n. 11, p. 967–970, https://doi.org/10.1130/G45276.1

Byerly, G. R., Kröner, A., Lowe, D. R., Todt, W., and Walsh, M. M., 1996, Prolonged magmatism and time constraints for sediment deposition in the early Archaean Barberton greenstone belt: evidence from the Upper Onverwacht and Fig Tree groups: Precambrian Research, v. 78, n. 1–3, p. 125–138, https://doi.org/10.1016/0301-9268(95)00073-9

Byerly, G. R., Lowe, D. R., and Heubeck, C., 2019, Geologic evolution of the Barberton Greenstone Belt – a unique record of crustal development, surface processes, and early life 3.55 to 3.20 Ga; *in* van Kranendonk, M. J., Bennett, V. C., and Hoffmann, J. E., editors, Earth's Oldest Rocks – Second Edition: Amsterdam, the Netherlands, Elsevier, p. 569–613, https://doi.org/10.1016/B978-0-444-63901-1.00024-1

Cumming, G. L., and Richards, J. R., 1975, Ore lead isotope ratios in a continuously changing earth: Earth and Planetary Science Letters, v. 28, n. 2, p. 155–171, https://doi.org/10.1016/0012-821X(75)90223-X

De Ronde, C. E. J., and Kamo, S. L., 2000, An Archaean arc–arc collisional event: a short-lived, (*ca.* 3 Myr) episode, Weltevreden area, Barberton Greenstone Belt, South Africa: Journal of African Earth Sciences, v. 30, n. 2, p. 219–248, https://doi.org/10.1016/S0899-5362(00)00017-8

de Vries, S. T., Nijman, W., and de Boer, P. L., 2010, Sedimentary geology of the Palaeoarchean Buck Ridge (South Africa) and Kittys Gap (Western Australia) volcano-sedimentary complexes: Precambrian Research, v. 183, n. 4, p. 749–769, https://doi.org/10.1016/j.precamres.2010.09.005

de Wit, M. J., 1991, Archaean greenstone belt tectonism and basin development: some insights from the Barberton and Pietersburg greenstone belts, Kaapvaal Craton, South Africa: Journal of African Earth Sciences (and the Middle East), v. 13, n. 1, p. 45–63, https://doi.org/10.1016/0899-5362(91)90043-X

Decker, N. B., Byerly, G. R., Stiegler, M. T., Lowe, D. R., and Stefurak, E., 2015, High resolution tephra and U/Pb chronology of the 3.33–3.26 Ga Mendon Formation, Barberton Greenstone Belt, South Africa: Precambrian Research, v. 261, p. 54–74, https://doi.org/10.1016/j.precamres.2015.02.003

Dickinson, W. R., and Gehrels, G. E., 2009, Use of U-Pb ages of detrital zircons to infer maximum depositional ages of strata: A test against a Colorado Plateau Mesozoic database: Earth and Planetary Science Letters, v. 288, n. 1–2, p. 115–125, https://doi.org/10.1016/j.epsl.2009.09.013

Diener, J. F. A., Stevens, G., Kisters, A. F. M., and Poujol, M., 2005, Metamorphism and exhumation of the basal parts of the Barberton greenstone belt, South Africa: Constraining the rates of Mesoarchaean tectonism: Precambrian Research, v. 143, n. 1–4, p. 87–112, https://doi.org/10.1016/j.precamres.2005.10.001

Drabon, N., and Lowe, D. R., 2021, Progressive accretion recorded in sedimentary rocks of the 3.28-3.23 Ga Fig Tree Group, Barberton Greenstone Belt: Geological Society of America Bulletin, https://doi.org/10.1130/B35973.1

Drabon, N., Lowe, D. R., Byerly, G. R., and Harrington, J. A., 2017, Detrital zircon geochronology of sandstones of the 3.6–.2 Ga Barberton greenstone belt: No evidence for older continental crust: Geology, v. 45, n. 9, p. 803–806, https://doi.org/10.1130/G39255.1

Drabon, N., Galic, A., Mason, P. R. D., and Lowe, D. R., 2019a, Provenance and tectonic implications of the 3.28–3.23 Ga Fig Tree Group, central Barberton greenstone belt, South Africa: Precambrian Research, v. 325, p. 1–19, https://doi.org/10.1016/j.precamres.2019.02.010

Drabon, N., Heubeck, C., and Lowe, D. R., 2019b, Evolution of an Archean fan delta and its implications for the initiation of uplift and deformation in the Barberton greenstone belt, South Africa: Journal of Sedimentary Research, v. 89, n. 9, p. 849–874, https://doi.org/10.2110/jsr.2019.46

Dunkl, I., Mikes, T., Frei, D., Gerdes, A., and von Eynatten, H., 2009, PepiAGE: data reduction program for time-resolved U/Pb analyses. Software manual: www.sediment.uni-goettingen.de/staff/dunkl/software

Dziggel, A., Stevens, G., Poujol, M., Anhaeusser, C. R., and Armstrong, R. A. 2002, Metamorphism of the granite-greenstone terrane south of the Barberton greenstone belt, South Africa: an insight into the tectono-thermal evolution of the lower portions of the Onverwacht Group: Precambrian Research, v. 114, n. 3–4, p. 221–247, https://doi.org/10.1016/S0301-9268(01)00225-X

Dziggel, A., Armstrong, R. A., Stevens, G., and Nasdala, L., 2005, Growth of zircon and titanite during metamorphism in the granitoid-greenstone terrain south of the Barberton greenstone belt, South Africa: Mineralogical Magazine, v. 69, n. 6, p. 1019–1036, https://doi.org/10.1180/0026461056960305

Eriksson, K. A., 1979, Marginal marine depositional processes from the Archaean Moodies Group, Barberton Mountain Land, South Africa: Evidence and significance: Precambrian Research, v. 8, n. 3–4, p. 153–182, https://doi.org/10.1016/0301-9268(79)90027-5

Frei, D., and Gerdes, A., 2009, Precise and accurate in situ U-Pb dating of zircon with high sample throughput by automated LA-SF-ICP-MS: Chemical Geology, v. 261, n. 3–4, p. 261–270, https://doi.org/10.1016/j.chemgeo.2008.07.025

Fuchs, S., Williams-Jones, A. E., and Przybyłowicz, W. J., 2016, The Origin of the Gold and Uranium Ores of the Black Reef Formation, Transvaal Supergroup, South Africa: Ore Geology Reviews, v. 72, p. 149–164, https://doi.org/10.1016/j.oregeorev.2015.07.010

Gamper, A., Heubeck, C., Demske, D., and Hoehse, M., 2012, Composition and microfacies of Archean microbial mats (Moodies Group, ca. 3.22 Ga, South Africa, *in* Noffke, N., and Chafetz, H., editors, Microbial Mats in Siliciclastic Depositional Systems Through Time: Society of Economic Paleontologists and Mineralogists Society for Sedimentary Geology, Tulsa, Special Publication, v. 101, p. 65–74, https://doi.org/10.2110/sepmsp.101.065

Gehrels, G., 2014, Detrital Zircon U-Pb Geochronology Applied to Tectonics: Annual Review of Earth and Planetary Sciences, v. 42, p. 127–149, https://doi.org/10.1146/annurev-earth-050212-124012

Gehrels, G., and Pecha, M., 2014, Detrital zircon U-Pb geochronology and Hf isotope geochemistry of Paleozoic and Triassic passive margin strata of western North America: Geosphere, v. 10, n. 1, p. 49–65, https://doi.org/10.1130/GES00889.1

Gehrels, G. E., Valencia, V. A., and Ruiz, J., 2008, Enhanced precision, accuracy, efficiency, and spatial resolution of U-Pb ages by laser ablation–multicollector–inductively coupled plasma–mass spectrometry: Geochemistry, Geophysics, Geosystems, v. 9, n. 3, p. Q03017, https://doi.org/10.1029/2007GC001805

Gerdes, A., and Zeh, A., 2006, Combined U-Pb and Hf isotope LA-(MC)ICP-MS analyses of detrital zircons: Comparison with SHRIMP and new constraints for the provenance and age of an Armorican metasediment in Central Germany: Earth and Planetary Science Letters, v. 249, n. 1–2, p. 47–61, https://doi.org/10.1016/j.epsl.2006.06.039

———, 2009, Zircon formation versus zircon alteration – new insights from combined U-Pb and Lu-Hf in-situ LA-ICP-MS analyses, and consequences for the interpretation of Archean zircon from the Central Zone of the Limpopo Belt: Chemical Geology, v. 261, n. 3–4, p. 230–243, https://doi.org/10.1016/j.chemgeo.2008.03.005

Gold, D. J. C., and von Veh, M. W., 1995, Tectonic evolution of the Late Archaean Pongola-Mozaan basin, South Africa: Journal of African Earth Sciences, v. 21, n. 2, p. 203–212, https://doi.org/10.1016/0899-5362(95)00069-6

Grosch, E. G., Kosler, J., McLoughlin, N., Drost, K., Slama, J., and Pedersen, R. B., 2011, Paleoarchean detrital zircon ages from the earliest tectonic basin in the Barberton Greenstone Belt, Kaapvaal craton, South Africa: Precambrian Research, v. 191, n. 1–2, p. 85–99, https://doi.org/10.1016/j.precamres.2011.09.003

Heinrichs, T., 1980, Lithostratigraphische Untersuchungen in der Fig Tree Gruppe des Barberton Greenstone Belt zwischen Umsoli und Lomati (Südafrika): Göttinger Arbeiten zur Geologie und Paläontologie, v. 22, 113 p.

Hellstrom, J., Paton, C., Woodhead, J., and Hergt, J., 2008, Iolite: Software for spatially resolved LA- (quad and MC) ICPMS analysis, *in* Sylvester, P., editor, Laser Ablation ICP–MS in the Earth Sciences: Current Practices and Outstanding Issues, Mineralogical Association of Canada, Quebec, Canada, p. 343–348.

Hessler, A. M., and Lowe, D. R., 2006, Weathering and sediment generation in the Archaean: An integrated study of the evolution of siliciclastic sedimentary rocks of the 3.2 Ga Moodies Group, Barberton Greenstone Belt, South Africa: Precambrian Research, v. 151, n. 3–4, p. 185–210, https://doi.org/10.1016/j.precamres.2006.08.008

Heubeck, C., 2009, An early ecosystem of Archean tidal microbial mats (Moodies Group, South Africa, ca. 3.2 Ga): Geology, v. 37, n. 10, p. 931–934, https://doi.org/10.1130/G30101A.1

———, 2019, The Moodies Group — a high-resolution archive of Archaean surface and basin-forming processes, *in* Kröner, A., and Hofmann, A., editors, The Archaean Geology of the Kaapvaal Craton, Southern Africa: Regional Geology Reviews, Springer, p. 133–169, https://doi.org/10.1007/978-3-319-78652-0_6

Heubeck, C., and Lowe, D. R., 1994, Depositional and tectonic Setting of the Archean Moodies Group, Barberton Greenstone Belt, South Africa: Precambrian Research, v. 68, n. 3–4, p. 257–290, https://doi.org/10.1016/0301-9268(94)90033-7

———, 1999, Sedimentary petrology and provenance of the Archean Moodies Group, Barberton Greenstone Belt, South Africa, *in* Lowe, D. R., and Byerly, G. R., editors, Geologic Evolution of the Barberton Greenstone Belt, South Africa: Geological Society of America Special Paper, v. 329, p. 259–286, https://doi.org/10.1130/0-8137-2329-9.259

Heubeck, C., Engelhardt, J., Byerly, G. R., Zeh, A., Sell, B., Luber, T., and Lowe, D. R., 2013, Timing of deposition and deformation of the Moodies Group (Barberton Greenstone Belt, South Africa): Very-high-resolution of Archaean surface processes: Precambrian Research, v. 231, p. 236–262, https://doi.org/10.1016/j.precamres.2013.03.021

Heubeck, C., Janse van Rensburg, D., Reimann, S., and Zametzer, A., 2020, Quartzofeldspathic Moodies Group sandstones (Barberton Greenstone Belt, ~3.22 Ga, South Africa and Eswatini) are derived from intra-BGB felsic igneous rocks, not from extra-BGB granites: Annual Meeting DGGV Utrecht, p. 24–26 August 2020, Utrecht, the Netherlands.

Hoffmann, J. E., and Kröner, A., 2018, Early Archaean crustal evolution in southern Africa—an updated record of the Ancient Gneiss Complex of Swaziland, *in* van Kranendonk, M. J., Bennett, V. C., and Hoffmann, J. E., editors, Earth's Oldest Rocks – Second Edition: Amsterdam, the Netherlands, Elsevier, p. 553–567, https://doi.org/10.1016/B978-0-444-63901-1.00023-X

Hoffmann, J. E., Kröner, A., Hegner, E., Viehmann, S., Xie, H., Iaccheri, L. M., Schneider, K. P., Hofmann, A., Wong, J., Geng, H., and Yang, J. H., 2016. Source composition, fractional crystallization and magma mixing processes of the 3.48–3.43 Ga Tsawela tonalite suite (Ancient Gneiss Complex, Swaziland)-implications for Palaeoarchean geodynamics: Precambrian Research, v. 276, p. 43–66, https://doi.org/10.1016/j.precamres.2016.01.026

Hoffmann, J. E., Musese, E., Kröner, A., Schneider, K. P., Wong, J., Hofmann, A., Hegner, E., Kasper, H. U., Tusch, J., and Münker, C., 2020, Hafnium-Neodymium isotope, trace element and U-Pb zircon age constraints on the petrogenesis of the 3.44–3.46 Ga Dwalile greenstone remnant, Ancient Gneiss Complex, Swaziland: Precambrian Research, v. 351, p. 105970, https://doi.org/10.1016/j.precamres.2020.105970

Homann, M., Heubeck, C., Airo, A., and Tice, M. M., 2015. Morphological adaptations of 3.22 Ga-old microbial mats to Archean coastal habitats (Moodies Group, Barberton Greenstone Belt, South Africa: Precambrian Research, v. 266, p. 47–64, https://doi.org/10.1016/j.precamres.2015.04.018

Ireland, T. R., and Williams, I. S., 2003, Considerations in zircon geochronology by SIMS: Reviews in Mineralogy and Geochemistry, v. 53, n. 1, p. 215–241, https://doi.org/10.2113/0530215

Jackson, M. P. A., Eriksson, K. A., and Harris, C. W., 1987, Early Archean foredeep sedimentation related to crustal shortening: a reinterpretation of the Barberton Sequence, southern Africa: Tectonophysics, v. 136, n. 3–4, p. 197–221, https://doi.org/10.1016/0040-1951(87)90025-4

Jackson, S. E., Pearson, N. J., Griffin, W. L., and Belousova, E. A., 2004, The application of laser ablation-inductively coupled plasma-mass spectrometry to in situ U-Pb zircon geochronology: Chemical Geology, v. 211, n. 1–2, p. 47–69, https://doi.org/10.1016/j.chemgeo.2004.06.017

Kamber, B. S., 2015, The evolving nature of terrestrial crust from the Hadean, through the Archaean, into the Proterozoic: Precambrian Research, v. 258, p. 48–82, https://doi.org/10.1016/j.precamres.2014.12.007

Kinny, P. D., 1986, 3820 Ma zircons from a tonalitic Armîsoq gneiss in the Godthåb district of southern West Greenland: Earth and Planetary Science Letters, v. 79, n. 3–4, p. 337–347, https://doi.org/10.1016/0012-821X(86)90190-1

Kisters, A. F. M., Stevens, G., Dziggel, A., and Armstrong, R. A., 2003, Extensional detachment faulting and core-complex formation in the southern Barberton granite-greenstone terrain, South Africa: evidence for a 3.2 Ga orogenic collapse: Precambrian Research, v. 127, n. 4, p. 355–378, https://doi.org/10.1016/j.precamres.2003.08.002

Kisters, A. F. M., Belcher, R. W., Poujol, M., and Dziggel, A., 2010, Continental growth and convergence-related arc plutonism in the Mesoarchaean: Evidence from the Barberton granitoid-greenstone terrain, South Africa: Precambrian Research, v. 178, n. 1–4, p. 15–26, https://doi.org/10.1016/j.precamres.2010.01.002

Knauth, L. P., and Lowe, D. R., 2003, High Archean climatic temperature inferred from oxygen isotope geochemistry of cherts in the 3.5 Ga Swaziland Supergroup, South Africa: Geological Society of America Bulletin, v. 115, n. 5, p. 566–580, https://doi.org/10.1130/0016-7606(2003)115<0566:HACTIF>2.0.CO;2

Kohler, E. A., and Anhaeusser, C. R., 2002, Geology and geodynamic setting of Archaean silicic metavolcaniclastic rocks of the Bien Venue Formation, Fig Tree Group, northeast Barberton greenstone belt, South Africa: Precambrian Research, v. 116, n. 3–4, p. 199–235, https://doi.org/10.1016/S0301-9268(02)00021-9

Kröner, A., and Compston, W., 1988, Ion microprobe ages of zircons from early Archean granite pebbles and greywacke, Barberton Greenstone Belt, Southern Africa: Precambrian Research, v. 38, p. 367–380, https://doi.org/10.1016/0301-9268(88)90034-4

Kröner, A., Compston, W., and Williams, I. S., 1989, Growth of early Archaean crust in the Ancient Gneiss Complex of Swaziland as revealed by single zircon dating: Tectonophysics, v. 161, n. 3–4, p. 271–298, https://doi.org/10.1016/0040-1951(89)90159-5

Kröner, A., Byerly, G. R., and Lowe, D. R., 1991, Chronology of early Archaean granite-greenstone evolution in the Barberton Mountain Land, South Africa, based on precise dating by single zircon evaporation: Earth and Planetary Science Letters, v. 103, n. 1–4, p. 41–54, https://doi.org/10.1016/0012-821X(91)90148-B

Kröner, A., Hoffmann, J. E., Xie, H., Wu, F., Münker, C., Hegner, E., Wong, J., Wan, Y., and Liu, D., 2013, Generation of early Archaean felsic greenstone volcanic rocks through crustal melting in the Kaapvaal, craton, southern Africa: Earth and Planetary Science Letters, v. 381, p. 188–197, https://doi.org/10.1016/j.epsl.2013.08.029

Kröner, A., Hoffmann, J. E., Xie, H., Münker, C., Hegner, E., Wan, Y., Hofmann, A., Liu, D., and Yang, J., 2014a, Generation of early Archaean grey gneisses through melting of older crust in the eastern Kaapvaal craton, southern Africa: Precambrian Research, v. 255, p. 823–846, https://doi.org/10.1016/j.precamres.2014.07.017

Kröner, A., Kovach, V., Belousova, E., Hegner, E., Armstrong, R., Dolgopolova, A., Seltmann, R., Alexeiev, D. V., Hoffmann, J. E., Wong, J., Sun, M., Cai, K., Wang, T., Tong, Y., Wilde, S. A., Degtyarev, K. E., and Rytsk, E., 2014b, Reassessment of continental growth during the accretionary history of the Central Asian Orogenic Belt: Gondwana Research, v. 25, n. 1, p. 103–125, https://doi.org/10.1016/j.gr.2012.12.023

Kröner, A., Anhaeusser, C. R., Hoffmann, J. E., Wong, J., Geng, H., Hegner, E., Xie, H., Yang, J., and Liu, D., 2016, Chronology of the oldest supracrustal sequences in the Palaeoarchaean Barberton Greenstone Belt, South Africa and Swaziland: Precambrian Research, v. 279, p. 123–143, https://doi.org/10.1016/j.precamres.2016.04.007

Kröner, A., Wong, J., and Xie, H., 2018a, The oldest granite clast in the Moodies conglomerate, Barberton greenstone belt, South Africa, and its likely origin: South African Journal of Geology, v. 121, n. 1, p. 43–50, https://doi.org/10.25131/sajg.121.0001

Kröner, A., Nagel, T. J., Hoffmann, J. E., Liu, X., Wong, J., Hegner, E., Xie, H., Kasper, U., Hofmann, A., and Liu, D., 2018b, High-temperature metamorphism and crustal melting at ca. 3.2 Ga in the eastern Kaapvaal craton, southern Africa: Precambrian Research, v. 317, p. 101–116, https://doi.org/10.1016/j.precamres.2018.08.007

Kröner, A., Hoffmann, J. E., Wong, J. M., Geng, H. Y., Schneider, K. P., Xie, H., Yang, J. H., and Nhleko, N., 2019, Archaean Crystalline Rocks of the Eastern Kaapvaal Craton , in Kröner, A., and Hofmann, A., editors, The Archaean Geology of the Kaapvaal Craton, Southern Africa: Regional Geology Reviews, Springer, Cambridge, p. 1–32, https://doi.org/10.1007/978-3-319-78652-0_1

Lamb, S. H, 1984, Structures on the eastern margin of the Archean Barberton greenstone belt, northwest Swaziland , in Kröner, A., and Greiling, R., editors, Precambrian Tectonics Illustrated, Final report/ International Union of Geological Sciences, Commission on Tectonics, Subcommission on Precambrian Structural Type Regions: Stuttgart, Germany, E. Schweizerbart'sche, p. 19–39.

Lamb, S., 1987, Archean synsedimentary tectonic deformation – A comparison with the Quaternary: Geology, v. 15, n. 6, p. 565–568, https://doi.org/10.1130/0091-7613(1987)15<565:ASTDCW>2.0.CO;2

Lamb, S., and Paris, I., 1988, Post-onverwacht stratigraphy in the southeastern part of the Archean Barberton Greenstone Belt: Journal of African Earth Sciences (and the middle East), v. 7, n. 1, p. 285–306, https://doi.org/10.1016/0899-5362(88)90074-7

Lana, C., Buick, I., Stevens, G., Roussow, R., and de Wet, W., 2011, 3230–3200 Ma post-orogenic extension and mid-crustal magmatism along the southeastern margin of the Barberton Greenstone Belt, South Africa: Journal of Structural Geology, v. 33, n. 5, p. 844–858, https://doi.org/10.1016/j.jsg.2011.03.007

Leisgang, I., ms, 2017, LA-ICP-MS zircon ages for clastic sediments of the Moodies Group, Barberton Greenstone Belt, South Africa and Swaziland. BSc thesis, Johannes-Gutenberg-University Mainz, Germany, 43 p.

Lowe, D. R., and Byerly, G. R., 1999, Stratigraphy of the west-central part of the Barberton Greenstone Belt, South Africa: Geological Society of America, Special Paper, v. 329, p. 1–36, https://doi.org/10.1130/0-8137-2329-9.1

———, 2020, The non-glacial and non-cratonic origin of an early Archean felsic volcaniclastic unit, Barberton Greenstone Belt, South Africa: Precambrian Research, v. 341, p. 105647, https://doi.org/10.1016/j.precamres.2020.105647

Lowe, D. R., Byerly, G. R., and Heubeck, C., 2012, Geologic Map of the west-central Barberton Greenstone Belt, South Africa: Boulder, Geological Society of America, Map and Chart Series 103, scale 1:25,000.

Lowe, D. R., Drabon, N., Byerly, G. R., and Byerly, B. L., 2021, Windblown Hadean zircons derived by erosion of impact-generated 3.3 Ga uplifts, Barberton Greenstone Belt, South Africa: Precambrian Research, v. 356, p. 106111, https://doi.org/10.1016/j.precamres.2021.106111

Luber, T., ms, 2012, Geology and geochronology of a marker tuff bed, Moodies Group, Stolzburg Syncline, Barberton Greenstone Belt, South Africa: B.Sc. thesis, Freie Universität Berlin, Berlin, Germany, p. 38

Ludwig, K. R., 2003, Isoplot/Ex Version 3.00, A Geochronological Toolkit for Microsoft Excel: Berkeley Geochronology Center Special Publication v. 4, 73 p.

———, 2009, Squid 2, A user's manual: Berkeley Geochronology Center Special Publication No. 5, 110 p.

———, 2011, User's manual for Isoplot/Ex: a geochronological toolkit for Microsoft Excel: Berkeley Geochronology Center

———, 2012, Isoplot 3.75, a geochronological toolkit for Excel: Berkeley Geochronology Center Special Publication, No. 5, 75 p.

Mojzsis, S. J., Harrison, T. M., and Pidgeon, R. T., 2001, Oxygen-isotope evidence from ancient zircons for liquid water at the Earth's surface 4,300 Myr ago: Nature, v. 409, p. 178–191, https://doi.org/10.1038/35051557

Moyen, J. F., Stevens, G., Kisters, A. F. M., and Belcher, B. L., 2018, TTG plutons of the Barberton Granitoid-Greenstone Terrain, South Africa , in van Kranendonk, M., Bennett, V., and Hoffmann, E., editors, Earth's Oldest Rocks – Second Edition: Amsterdam, The Netherlands, Elsevier, p. 607–667.

Moyen, J. F., Zeh, A., Cuney, M., Dziggel, A., and Carrouée, S., 2021, The multiple ways of recycling Archaean crust: a case study from the *ca.* 3.1 Ga "late" granitoids from the Barberton Greenstone Belt, South Africa: Precambrian Research, v. 353, 105998, https://doi.org/10.1016/j.precamres.2020.105998

Nasdala, L., Hofmeister, W., Norberg, N., Martinson, J. M., Corfu, F., Dörr, W., Kamo, S. L., Kennedy, A. K., Kronz, A., Reiners, P. W., Frei, D., Kosler, J., Wan, Y., Götze, J., Häger, T., Kröner, A., and Valley, J. W., 2008, Zircon M257 - A homogeneous natural reference material for the ion Microprobe U-Pb analysis of Zircon: Geostandards and Geoanalytical Research, v. 32, n. 3, p. 247–265, https://doi.org/10.1111/j.1751-908X.2008.00914.x

Nelson, D. R., 1997, Compilation of SHRIMP U-Pb zircon geochronology data, 1996: Geological Survey of Western Australia, Record 1997/2, 189 p.

Olsson, J. R., Söderlund, U., Klausen, M. B., and Ernst, R. E., 2010, U-Pb baddeleyite ages linking major Archean dyke swarms to volcanic-rift forming events in the Kaapvaal craton (South Africa), and a precise age for the Bushveld Complex: Precambrian Research, v. 183, n. 3, 490–500, https://doi.org/10.1016/j.precamres.2010.07.009

Paces, J. B., and Miller, J. D. Jr., 1993, Precise U-Pb ages of Duluth complex and related mafic intrusions, northeastern Minnesota: Geochronological insights to physical, petrogenetic, paleomagnetic, and tectonomagmatic processes associated with the 1.1 Ga midcontinent rift system: Journal of Geophysical Research: Solid Earth, v. 98, n. B8, p. 13997–14013, https://doi.org/10.1029/93JB01159

Paton, C., Woodhead, J. D., Hellstrom, J. C., Hergt, J. M., Greig, A., and Maas, R., 2010, Improved laser ablation U-Pb zircon geochronology through robust downhole fractionation correction: Geochemistry Geophysics Geosystems, v. 11, n. 3, p. 1–36, https://doi.org/10.1029/2009GC002618

Paton, C., Hellstrom, J., Paul, B., Woodhead, J., and Hergt, J., 2011, Iolite: Freeware for the visualisation and processing of mass spectrometric data: Journal of Analytical Atomic Spectrometry, v. 26, n. 12, p. 2508–2518, https://doi.org/10.1039/c1ja10172b

Petrus, J. A., and Kamber, B. S., 2012, VizualAge: A Novel Approach to Laser Ablation ICP-MS U-Pb Geochronology Data Reduction: Geostandards and Geoanalytical Research, v. 36, n. 3, p. 247–270, https://doi.org/10.1111/j.1751-908X.2012.00158.x

Reimann, S., Heubeck, C., Janse van Rensburg, D. J., Fugmann, P., Serre, S. H., Thomsen, T. B., and Zametzer, A., 2021, Syndepositional hydrothermalism selectively preserves records of one of the earliest benthic ecosystems, Moodies Group (3.22 Ga), Barberton Greenstone Belt, South Africa: South African Journal of Geology, v. 124, n. 1, p. 253–278, https://doi.org/10.25131/sajg.124.0012

Reimer, T. O., ms, 1967, Die Geologie der Stolzburg-Synklinale im Barberton Bergland (Transvaal-Südafrika): Diplomarbeit, Goethe-Universität Frankfurt/Main, 136 p.

Sanchez-Garrido, C. J. M. G., Stevens, G., Armstrong, R. A., Moyen, J.-F., Martin, H., and Doucelance, R., 2011, Diversity in Earth's early felsic crust: Paleoarchean peraluminous granites of the Barberton Greenstone Belt: Geology, v. 39, n. 10, p. 963–966, https://doi.org/10.1130/G32193.1

Schmitz, M., and Heubeck, C., 2021, Constraints on deformation mechanisms of the Barberton Greenstone Belt from regional stratigraphic and structural data of the synorogenic Moodies Group: Precambrian Research, v. 362, 106177, https://doi.org/10.1016/j.precamres.2021.106177

Schmitz, M. D., Bowring, S. A., and Ireland, T. R., 2003, Evaluation of Duluth Complex anorthositic series (AS3) zircon as a U-Pb geochronological standard: New high-precision isotope dilution thermal ionization mass spectrometry results: Geochimica et Cosmochimica Acta, v. 67, n. 19, p. 3665–3672, https://doi.org/10.1016/S0016-7037(03)00200-X

Sharman, G. R., Sharman, J. P., and Sylvester, Z., 2018, DetritalPy: A Python-based Toolset for Visualizing and Analyzing Detrital Geo-Thermochronologic Data: The Depositional Record, v. 4, n. 2, p. 202–215, https://doi.org/10.1002/dep2.45

Sláma, J., Košler, J., Condon, D. J., Crowley, J. L., Gerdes, A., Hanchar, J. M., Horstwood, M. S. A., Morris, G.A., Nasdala, L., Norberg, N., Schaltegger, U., Schoene, B., Tubrett, M. N., and Whitehouse, M. J., 2008, Plešovice zircon - A new natural reference material for U-Pb and Hf isotopic microanalysis: Chemical Geology, v. 249, n. 1–2, p. 1–35, https://doi.org/10.1016/j.chemgeo.2007.11.005

Stacey, J. S., and Kramers, J. D., 1975, Approximation of terrestrial lead isotope evolution by a two-stage model: Earth and Planetary Science Letters, v. 26, n. 2, p. 207–221, https://doi.org/10.1016/0012-821X(75)90088-6

Stern, R. A., Bodorkos, S., Kamo, S. L., Hickman, A. H., and Corfu, F., 2009, Measurement of SIMS instrumental mass fractionation of Pb isotopes during zircon dating: Geostandards and Geoanalytical Research, v. 33, n. 2, p. 145–168, https://doi.org/10.1111/j.1751-908X.2009.00023.x

Stoll, E., Drabon, N., and Lowe, D. R., 2021, Provenance and paleogeography of Archean Fig Tree siliciclastic rocks in the East-Central Barberton Greenstone Belt, South Africa: Precambrian Research, v. 354, 106041, https://doi.org/10.1016/j.precamres.2020.106041

Stutenbecker, L., Heubeck, C., and Zeh, A., 2019, The Lomati Delta Complex: A prograding tidal delta in the Archean Moodies Group, Barberton Greenstone Belt: South African Journal of Geology, v. 122, n.1, p. 17–38, https://doi.org/10.25131/sajg.122.0002

Taylor, J., Zeh, A., and Gerdes, A., 2016, U-Pb-Hf-isotope systematics of detrital zircons in high-grade paragneisses of the Ancient Gneiss Complex, Swaziland: evidence for two periods of juvenile crust formation, Paleo- and Mesoarchaean sediment deposition, and 3.23 Ga terrane accretion: Precambrian Research, v. 280, p. 205–220, https://doi.org/10.1016/j.precamres.2016.05.012

Tegtmeyer, A., and Kröner, A., 1987, U-Pb zircon ages bearing on the nature of early Archaean greenstone belt evolution, Barberton Mountainland, southern Africa: Precambrian Research, v. 36, n. 1, p. 1–20, https://doi.org/10.1016/0301-9268(87)90014-3

Tice, M. M., Bostick, B. C., and Lowe, D. R., 2004, Thermal history of the 3.5–3.2 Ga Onverwacht and Fig Tree Groups, Barberton greenstone belt, South Africa, inferred by Raman microspectroscopy of carbonaceous material: Geology, v. 32, n. 1, p. 37–40, https://doi.org/10.1130/G19915.1

Toulkeridis, T., Goldstein, S. L., Clauer, N., Kröner, A., Todt, W., and Schidlowski, M., 1998, Sm–Nd, Rb–Sr and Pb–Pb dating of silicic carbonates from the early Archaean Barberton Greenstone Belt, South Africa: Evidence for post-depositional isotopic resetting at low temperature: Precambrian Research, v. 92, n. 2, p. 129–144, https://doi.org/10.1016/S0301-9268(98)00071-0

Urie, J. G., 1970, Geological map series Sheet 3, Forbes Reef: Swaziland Geological Survey and Mines Department, Mbabane, scale 1:25,000.

——, 1971, Geological Map Series Sheet 4, Motshane: Swaziland Geological Survey and Mines Department, Mbabane, scale 1:25,000.

Valley, J. W., Peck, W. H., King, E. M., and Wilde, S. A., 2002, A cool early Earth: Geology, v. 30, n. 4, p. 351–354, https://doi.org/10.1130/0091-7613(2002)030<0351:ACEE>2.0.CO;2

Valley, J. W., Lackey, J. S., Cavosie, A. J., Clechenko, C. C., Spicuzza, M. J., Basei, M. A. S., Bindeman, I. N., Ferreira, V. P., Sial, A. N., King, E. M., Peck, W. H., Sinha, A. K., and Wei, C. S., 2005, 4.4 billion years of crustal maturation: Oxygen isotope ratios of magmatic zircon: Contributions to Mineralogy and Petrology, v. 150, p. 561–580, https://doi.org/10.1007/s00410-005-0025-8

Van Kranendonk, M. J., 2011, Cool greenstone drips and the role of partial convective overturn in Barberton greenstone belt evolution: Journal of African Earth Sciences, v. 60, n. 5, p. 346–352, https://doi.org/10.1016/j.jafrearsci.2011.03.012

Van Kranendonk, M. J., Kröner, A., Hegner, E., and Connelly, J., 2009, Age, lithology and structural evolution of the c. 3.53 Ga Theespruit Formation in the Tjakastad area, southwestern Barberton Greenstone Belt, South Africa, with implications for Archean tectonics: Chemical Geology, v. 261, n. 1–2, p. 115–139, https://doi.org/10.1016/j.chemgeo.2008.11.006

Van Kranendonk, M. J., Kröner, A., Hoffman, J. E., Nagel, T., and Anhaeusser, C. R., 2014, Just another drip: Re-analysis of a proposed Mesoarchean suture from the Barberton Mountain Land, South Africa: Precambrian Research, v. 254, p. 19–35, https://doi.org/10.1016/j.precamres.2014.07.022

Van Kranendonk, M., Bennett, V., and Hoffmann, E., editors 2018, Earth's oldest rocks: Elsevier, 1112 p.

Van Niekerk, C. B., and Burger, A. J., 1978, The age of the Moodies conglomerate boulders: Geological Society of South Africa Special Publication, v. 4, p. 99–106

van Schijndel, V., Stevens, G., Zeh, A., Frei, D., and Lana, C., 2017, Zircon geochronology and Hf isotopes of the Dwalile Supracrustal Suite, Ancient Gneiss Complex, Swaziland; Insights into the diversity of Paleoarchean source rocks, depositional and metamorphic ages: Precambrian Research, v. 295, p. 48–66, https://doi.org/10.1016/j.precamres.2017.04.025

Vermeesch, P., 2012, On the visualisation of detrital age distributions: Chemical Geology, v. 312–313, p. 190–194, https://doi.org/10.1016/j.chemgeo.2012.04.021

Wang, H., Yang, J.-H., Kröner, A., Zhu, Y.-S., and Li, R., 2019, Non-subduction origin for 3.2 Ga high-pressure metamorphic rocks in the Barberton granitoid-greenstone terrane, South Africa: Terra Nova, v. 31, n. 4, p. 373–380, https://doi.org/10.1111/ter.12397

Wiechert, A., ms, 2014, Contributions to the geochronology of the northern and southern facies of the Archean Moodies Group (Barberton Greenstone Belt, South Africa and Swaziland): M.Sc. thesis, Freie Universität Berlin, Berlin, Germany, 81 p.

Wiedenbeck, M., Allé, P., Corfu, F., Griffin, W. L., Meier, M., Oberli, F., von Quadt, A., Roddick, J. C., and Spiegel, W., 1995, Three natural zircon standards for U-Th-Pb, Lu-Hf, trace element and REE analyses: Geostandards Newsletter, v. 19, n. 1, p. 1–23, https://doi.org/10.1111/j.1751-908X.1995.tb00147.x

Wiedenbeck, M., Hanchar, J. M., Peck, W. H., Sylvester, P., Valley, J., Whitehouse, M., Kronz, A., Morishita, Y., Nasdala, L., Fiebig, J., Franchi, I., Girard, J.-P., Greenwood, R. C., Hinton, R., Kita, N., Mason, P. R. D., Norman, M., Ogasawara, M., Piccoli, P. M., Rhede, D., Satoh, H., Schulz-Dobrick, B., Skår, Ø., Spicuzza, M. J., Terada, K., Tindle, A., Togashi, S., Vennemann, T., Xie, Q., and Zheng, Y.-F., 2004, Further characterisation of the 91500 zircon crystal: Geostandards and Geoanalytical Research, v. 28, n. 1, p. 9–39, https://doi.org/10.1111/j.1751-908X.2004.tb01041.x

Wilde, S. A., Valley, J. W., Peck, W. H., and Graham, C. M., 2001, Evidence from detrital zircons for the existence of continental crust and oceans on the Earth 4.4 Gyr ago: Nature, v. 409, p. 175–178, https://doi.org/10.1038/35051550

Williams, I. S., 1997, U-Th-Pb geochronology by ion microprobe, in Applications of microanalytical techniques to understanding mineralizing processes: Society of Economic Geologists Reviews in Economic Geology, v. 7, p. 1–35, https://doi.org/10.5382/Rev.07.01

Xie, X., Byerly, G. R., and Ferrell, R. E., 1997, IIb trioctahedral chlorite from the Barberton greenstone belt: crystal structure and rock composition constraints with implications to geothermometry: Contributions to Mineralogy and Petrology, v. 126, p. 275–291, https://doi.org/10.1007/s004100050250

Zametzer, A., ms, 2019, Geology of the Archean Powerline Road Syncline region, central Barberton Greenstone Belt, South Africa: M.Sc. thesis, Friedrich Schiller University, Jena, Germany, 171 p.

Zeh, A., Gerdes, A., and Barton, J. M., 2009, Archean accretion and crustal evolution of the Kalahari Craton—the zircon age and Hf isotope record of granitic rocks from Barberton/Swaziland to the Francistown Arc: Journal of Petrology, v. 50, n. 5, p. 933–966, https://doi.org/10.1093/petrology/egp027

Zeh, A., Gerdes, A., Barton, J. M., and Klemd, R. 2010, U-Th-Pb and Lu-Hf systematics of zircon from TTG's, leucosomes, meta-anorthosites and quartzites of the Limpopo Belt (South Africa): constraints for the formation, recycling, and metamorphism of Paleoarchean crust: Precambrian Research, v. 179, n. 1–4, p. 50–68, https://doi.org/10.1016/j.precamres.2010.02.012

Zeh, A., Gerdes, A., and Millonig, L., 2011, Hafnium isotope record of the Ancient Gneiss Complex, Swaziland, southern Africa: evidence for Archaean crust–mantle formation and crust reworking between 3.66 and 2.73 Ga: Journal of the Geological Society of London, v. 168, p. 953–964, https://doi.org/10.1144/0016-76492010-117

Zeh, A., Gerdes, A., and Heubeck, C., 2013, U-Pb and Hf isotope data of detrital zircons from the Barberton Greenstone Belt: Constraints on provenance and Archaean crustal evolution: Journal of the Geological Society of London, v. 170, p. 215–223, https://doi.org/10.1144/jgs2011-162

Zeh, A., Wilson, A. H., and Gerdes, A., 2020, Zircon U-Pb-Hf isotope systematics of Transvaal Supergroup – Constraints for the geodynamic evolution of the Kaapvaal Craton and its hinterland between 2.65 and 2.06 Ga: Precambrian Research, v. 345, 105760, https://doi.org/10.1016/j.precamres.2020.105760